
Electrical Engineering Department

California Polytechnic State University, San Luis Obispo

Senior Project Report

# Miniaturized Ultraviolet Imager High Voltage Power Supply

by

Nicholas Palmer

Jason Heil

Dr. Taufik

June 2021

# Table of Contents

# List of Figures

# List of Tables

# Abstract

Sending satellites into orbit becomes exponentially more expensive with weight and size, so designing high-voltage DC-DC converters that can achieve kilovolt level outputs in a small form factor is crucial to reducing costs. The Miniaturized Ultraviolet Imager (MUVI) aims to monitor Earth's ionosphere and report weather patterns to climate scientists within a 2U cube satellite footprint. The imaging equipment consists of a microchannel plate and phosphor screen that require 2.5kV and 5.5kV respectively at microamp level currents. This report explains the implementation of a high voltage boost cascaded flyback converter to meet all of the MUVI satellite output voltage requirements.

The small mechanical footprint of a cube satellite severely limits board size and component heights. This design further expands the power electronics field and provides inspiration for future space-rated voltage converters in small form factors.

The results from circuit simulations validated the design as a viable solution for MUVI's imaging equipment. A boost-flyback converter can achieve the required high voltage DC output while remaining within the 7ppm ripple specification. This report summarizes all of the circuit simulation results for both the power stage and analog circuitry that monitor and control the output voltage. The analog circuitry was hardware tested and validated for the monitoring and control signals. The power stage testing is scheduled for the Summer of 2021 so those results are not included in this report.

# Chapter 1 – Introduction

Most modern-day devices require some form of electricity. All household appliances, smartphones, and cars contain components that consume electrical power from different types of sources. High voltage AC from utility providers supplies household appliances while low voltage DC from batteries supplies smartphones and cars. In either case, the input power is efficiently converted into usable voltages and currents to operate integrated circuits and other components within a device.

The technology used to convert electrical power from a source to a form that is useable by the load is called power electronics. More specifically, power electronics is the study of efficiently converting electric energy by controlling solid-state electronic devices like MOSFETs and BJTs [1]. The history of power electronics dates back to 1902 when Peter Cooper Hewitt invented the mercury-arc valve which rectified high-voltage or high-current AC to DC [2]. Mercury-arc rectifiers provided power for motors, railways, streetcars, electric locomotives, and high-voltage direct current (HVDC) power transmission. The field of power electronics and its applications skyrocketed when the first silicon transistor was invented in 1948 and the first silicon-controlled rectifier (SCR) was invented in 1954 by Bell Laboratories [3]. Since then, power electronics has improved the function and power efficiency of electronic devices in every corner of the electrical engineering industry.

Within the field of power electronics there are four main types of power converters consisting of AC-AC, AC-DC, DC-AC, and DC-DC. An AC-AC converter changes an AC source with a fixed voltage and frequency to a variable voltage and frequency. A common application of AC-AC converters are dimmer switches for house lighting. A switching circuit is used to lower the root mean square (RMS) voltage before passing it to the load. AC-DC

converters are widely used because our power grid supplies AC power, however many electrical loads require a DC supply for operation. A phone charger demonstrates a common AC-DC converter. The device rectifies the high voltage AC source to a low voltage DC output capable of charging the phone's battery. DC-AC converters, more commonly called inverters, convert a fixed DC voltage into a variable AC voltage and frequency. Electric vehicles commonly use DC-AC converters to convert the DC voltage from large batteries to a variable voltage AC output capable of driving induction motors. The DC-DC converter is another widely used converter capable of emulating a step-up or step-down DC transformer. A complicated device like a video camera contains many integrated circuits that may require different DC voltages to operate. The camera has one DC source in the form of a battery. Therefore, the camera employs DC-DC converters to step-up or step-down the battery voltage to supply each IC with their respective power requirements.

A DC-DC converter circuit can be implemented in two different ways: non-isolated and isolated. Non-isolated converters have electrically connected feedback between the input and output of the system. Isolated converters employ transformers and opto-couplers to prevent an electrical connection from the input to the output while still providing feedback to the controller. The category of non-isolated DC-DC converters contains three main topologies: boost, buck, and buck-boost converters. The boost converter acts as a step-up DC transformer that can output a higher voltage than its input. The buck converter acts as a step-down DC transformer that outputs a lower voltage than its input. The buck-boost converter has the ability to step-up or step-down DC voltages and is constructed by combining the first two topologies. The category of isolated DC-DC converters contains three main topologies: push-pull, single-switch forward, and flyback. The push-pull converter uses two switches, two diodes, and one center-tapped transformer to step-up and step-down DC voltages. The single-switch forward converter utilizes one switch, three transformer windings, and two diodes to step-up and step-down DC voltages.

The flyback converter uses one switch, one diode, and one transformer to step-up and step-down DC voltages. Each topology has strengths and weaknesses that can be leveraged when approaching design problems. Important considerations are input noise, output noise, size, complexity, and cost.

Power electronic devices such as DC-DC converters can be found in a wide variety of applications like renewable energy, power distribution, transportation, and space exploration. DC-DC converters in particular have also been studied for use in many unique applications. At Cal Poly for example, there have been studies conducted on DC-DC converters for use to combine multiple renewable energy sources into a single DC bus [4-6], to distribute residential DC power [7][8], and to power low-voltage high current devices [9]. In addition, another exciting DC-DC converter application that is currently being studied is for space application which produces high voltage output.

# Chapter 2 – Background

As space technologies increase in complexity yet reduce in size and cost, the need for specialized DC power converters increases. These converters need to supply power to the various onboard instruments and gauges at specific voltages and currents. One drawback of DC-DC converters is voltage and current ripple at the input and output due to using a switch to rapidly connect and disconnect the load and storage elements from the source. The switching noise is undesirable when converting and delivering power but is seen as a worthwhile tradeoff for improved efficiency over using a linear voltage regulator. Luckily, the use of filters and intelligent switching methods can decrease the amount of noise found on the input and output of these converters. The following examples showcase ingenuity for creating space-related DC-DC converters that can produce high voltages in a small package.

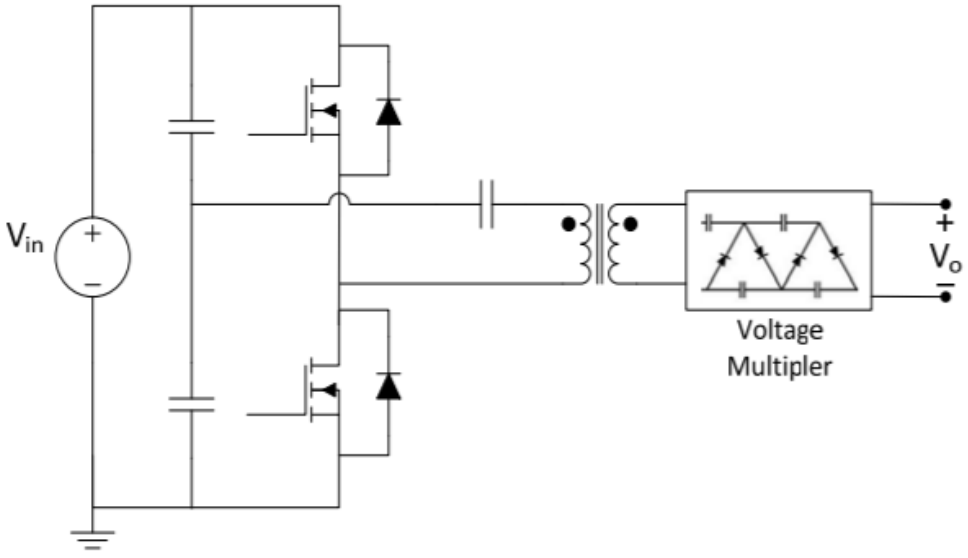


*Figure 2-1: Power stage of Series Loaded Resonant Converter with voltage multiplier [11]*

One example of a high voltage DC-DC converter used in a space application concerns the master's thesis of Nicholas Weiser from 2014. In his thesis, Nicholas created a DC-DC converter

capable of boosting a 9V supply to 5,000V. The high voltage converter supplied power to an Ion-Spray propulsion system capable of pushing a CubeSat from Low Earth Orbit (LEO) towards interplanetary travel [11]. After forming a table listing the advantages and disadvantages of various topologies, Nicholas chose to design a Series-Loaded Resonant Converter (SLR converter) operating in discontinuous conduction mode (DCM). The SLR converter is shown in Figure 2-1. Some advantages associated with an SLR converter include the ability for soft-switching to increase efficiency while reducing noise, the flexibility to use a small two-winding transformer, and the ability to use slow switching diodes. Operating the circuit in DCM inherently provides short circuit protection without adding extra components to the circuit [10].

Another example of a space specific application comes from an IEEE article written by Alan Weinberg and Jan Schreuders that explains the operation of a high-power DC-DC converter used to supply a mercury-iron motor for the Asteroid Gravity Optical and Radar Analysis (AGORA) mission [12]. This DC-DC converter deals with high-voltage and high-power through a buck-fed push-pull topology. Some advantages of this topology include forced current sharing, phase synchronized modules, low turns ratio transformers (1:3), and output diodes not requiring high reverse breakdown voltages. Another advantage of going for cascaded converters is that the buck stage can control the peak current being fed into the push-pull converter. Due to operating in a vacuum the main concern is efficiency to reduce heat generation. The design was optimized to reduce dynamic switching losses by using a turn-off snubber on the buck stage, seen in Figure 2-2. The snubber consists of diodes, capacitors, and an inductor connected to the MOSFET switch to create a resonant circuit which stores and releases energy out of phase with the switching signal to reduce voltage across and current through the switch when it turns off.

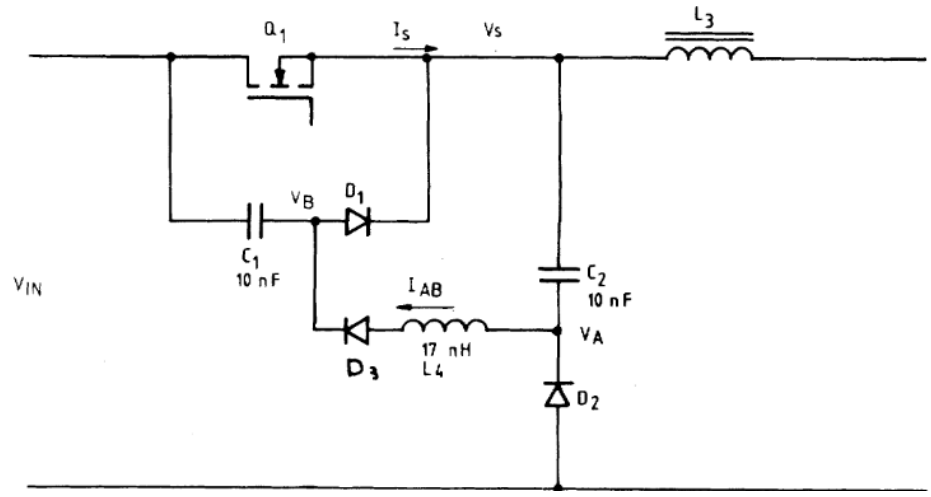


*Figure 2-2: Circuit diagram for the LCD energy recovery snubber for buck converters [12]*

A similar topology was found in an IEEE article by Qiang Tong and Donglai Zhang showing research into a DC-DC converter topology called the "cascaded buck, current fed push-pull converter" aimed at supplying a high output current over a wide range of input voltages [13]. This topology allows the circuit to be powered by solar panels that provide a wide voltage range. The DC-DC converter aims to provide a steady 28V or 42V output with high current capability. The rest of the satellite can draw power off the bus voltage that the DC-DC converter creates. The article details the design, testing, and analysis of the new converter topology. The Buck Converter makes up the regulating stage and is powered by a DC source with a wide input voltage range such as a solar panel. The Buck Converter provides a constant current at its output which is fed into the input of the constant current fed Push-Pull Converter. The output of the second stage is then rectified and filtered to the requirements of the voltage bus. The proposed topology also uses magnetic coupling to the output voltage to provide a more radiation tolerant solution of delivering isolated feedback to the converter's controller.

Focusing on a size efficient design, engineers at Stanford University were able to create a "small and lightweight high-voltage high-gain power converter" by "driving a Dickson and Cockroft-Walton voltage multiplier using a megahertz-frequency class-E inverter." [14]. One

converter scales 40 volts to 2,000V in a volume of 16 $cm^3$ and another converter scales 3.7V to 2,900V in a volume of 0.2 $cm^3$. The main idea for reducing the size of these DC-DC converters is to also decrease the weight and reduce the cost of sending the satellite to space. The inverter stage converts the DC voltage input into an AC voltage output before feeding into the Dickson Charge Pump voltage multiplier, seen in Figure 2-3. The voltage multiplier is a space and energy efficient voltage booster that leverages a capacitor and diode ladder which charges alternating stages on each cycle of the AC input. The only power loss in a voltage multiplier comes from the small resistances found in the capacitors, diodes, and PCB traces. The volume of these converters could be shrunk down by increasing the number of stages found in the voltage multiplier. In one voltage multiplier they constructed 55 stages to increase the output voltage 55 times higher than the input voltage.

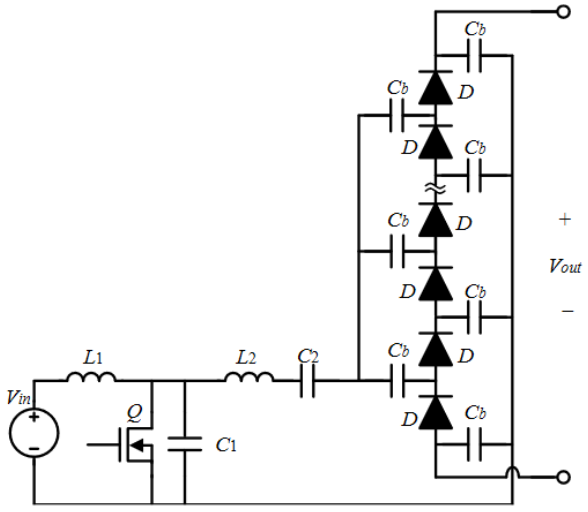


*Figure 2-3: Circuit diagram of a DC-AC inverter cascaded to an LC filter and then a Dickson Charge Pump voltage multiplier [14]*

Another example of a high voltage DC-DC converter used in space is located on the Ionosphere Connection Explorer (ICON). ICON collects data from a charged region of the atmosphere called the Ionosphere. Scientists use the information to predict how solar forces and Earth's weather systems. The DC-DC converter on ICON provides power to a Microchannel

Plate (MCP) and Phosphor Screen. The system boosts a 13V input to 3,000V and 6,000V for the MCP and Phosphor Screen respectively [15]. The large voltage step-up required the use of a two-stage converter. The first stage contains a push-pull converter that utilizes a transformer and BJTs to step-up the input voltage. The second stage uses a Cockcroft-Walton Multiplier to further increase the output voltage. The push-pull converter provided an output voltage waveform with a large peak to peak value. The multiplier increases the voltage and rectifies it to a DC value. The multiplier provides an effective way to provide a steady, filtered DC voltage.

The Miniaturized Ultraviolet Imager (MUVI) will replace the outdated ICON satellites. MUVI will perform the same functions as ICON such as data collection from the Ionosphere of Earth. The Ionosphere contains particles that have been charged by the Sun. These particles cause electromagnetic interference (EMI) that can wreak havoc on sensitive electronics equipment found on Earth. Since technology pervades almost every aspect of human life, we must have the capability to predict when such interferences can occur or risk the destruction of systems that are vital to our society's way of life. MUVI aims to be a smaller, more cost-effective satellite than ICON. Since it is smaller and less expensive, multiple MUVI satellites will be sent to space to monitor a larger portion of Earth's Ionosphere simultaneously. Since ICON's high voltage power supply (HVPS) is approximately the size of the entire MUVI satellite, the HVPS must be redesigned. The aim of this project is to design, build, and test a HVPS that satisfies that can survive the harsh conditions of space while meeting the electrical and physical requirements of MUVI.

# Chapter 3 – Design Requirements

Before designing the high voltage power supply, design requirements and validation criteria are required. The following design requirements were given by the sponsor at UC Berkeley to ensure the high voltage power supply provides the correct voltages and currents to the microchannel plate and phosphor screen, while remaining within a small physical envelope suitable for a cube satellite. The high voltage power supply must provide a separate DC output for the microchannel plate and the phosphor screen. The power source for the system is a 13V (±5%) DC bus provided by the instrument control package and the entire system must consume less than 1W of power. The microchannel plate requires 2.5 kV (±1%) and up to 50µA of current while the phosphor screen requires 5.5 kV (±1%) and up to 2µA of current. In addition to DC outputs the power supply must also provide voltage, current, and temperature monitoring information back to the instrument control package in the form of variable DC voltage. The Level 0 block diagram in Figure 3-1 provides a summary of inputs and outputs for this system.

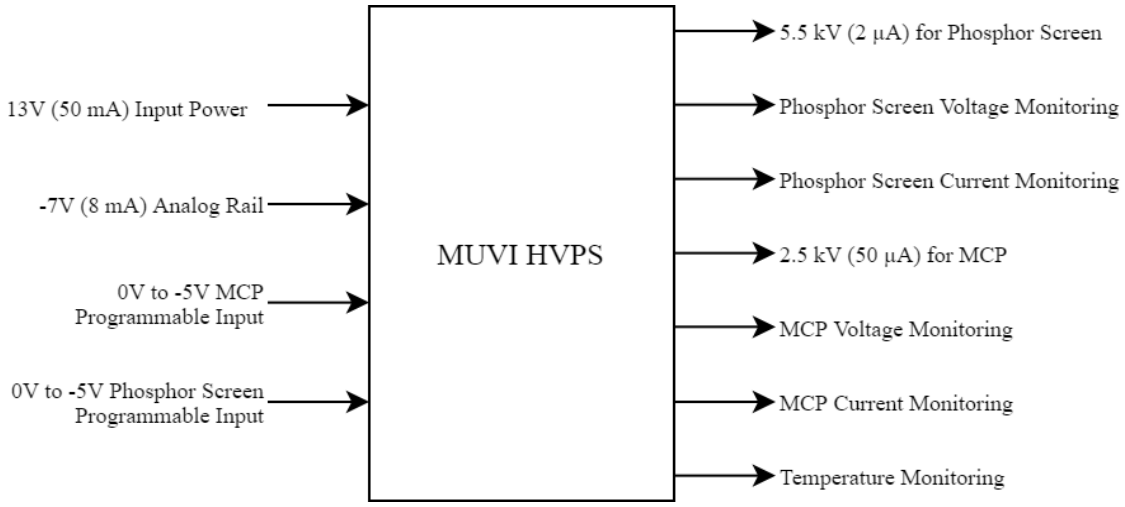


*Figure 3-1: Level 0 block diagram for the MUVI high voltage power supply*

TABLE 3-1: LEVEL 0 BLOCK DIAGRAM EXPLANATION

| **Module** | MUVI High Voltage Power Supply |
|---|---|
| **Inputs** | ● 13V (50mA) input power<br>● -7V (8mA) analog rail<br>● 0V to -5V MCP and Phosphor Screen Programmable Inputs |
| **Outputs** | ● 5.5 kV (2µA) output for Phosphor Screen<br>● Phosphor Screen Voltage and Current Monitoring Signals<br>● 2.5kV (50µA) output for Microchannel Plate<br>● Microchannel Plate Voltage and Current Monitoring Signals<br>● Temperature Monitoring Signal |
| **Functionality** | To scale the low input voltage to high output voltages for the phosphor screen and microchannel plate while providing output monitoring feedback |

The microchannel plate and phosphor screen have individual programmable inputs to independently control each output voltage. The programmable input maps linearly to the output voltages so 0V input corresponds to 0% output voltage and -5V input corresponds to 100% output voltage. Safe operation of the phosphor screen requires maintaining a 3 kV bias above the microchannel plate at all times. This is achieved during initial startup by increasing the phosphor screen's output voltage to 3 kV and then slowly ramping up the phosphor screen and microchannel plate by 2.5 kV together. Lastly the -7V analog rail provides a negative voltage for using op-amps in the monitoring circuits.

DC-DC converters are high power density systems capable of delivering thousands of volts at low current as seen in the examples in Chapter 2. To take advantage of this fact a DC-DC converter was chosen to meet all the power delivery specifications. The level 1 block diagram in Figure 3-2 shows a general outline of the different systems planned for the high voltage power supply. The microchannel plate and phosphor screen function the same way so both systems use the same types of modules for power, control, and monitoring.

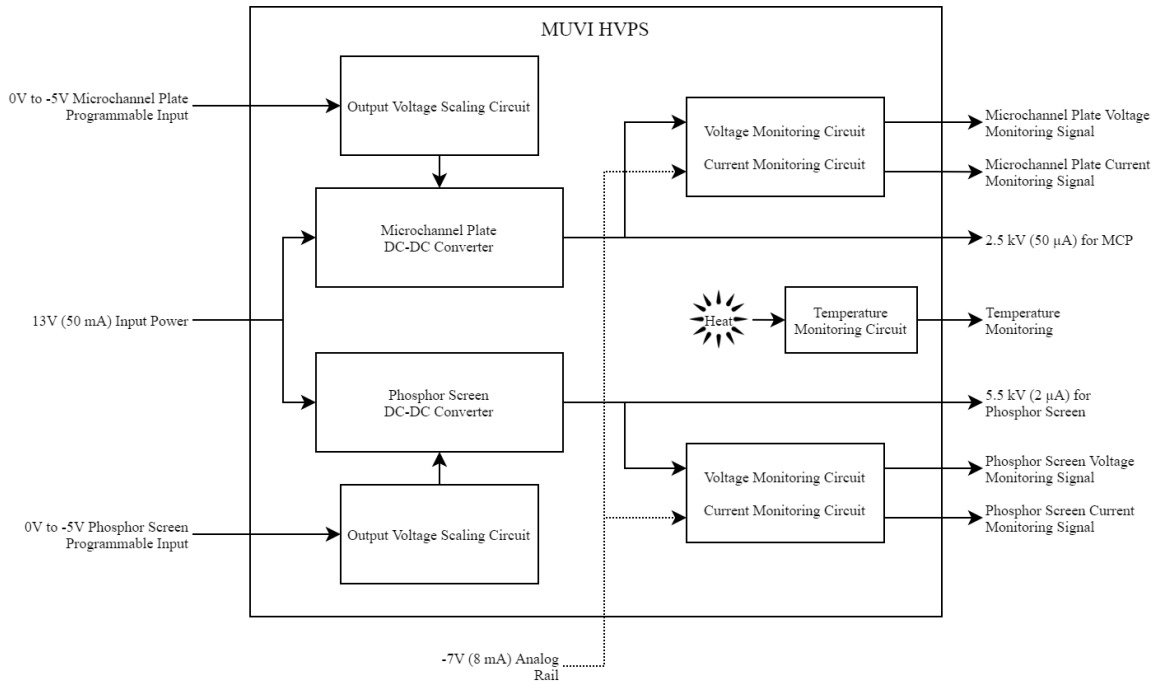


*Figure 3-2: Level 1 block diagram for the MUVI high voltage power supply*

TABLE 3-2: LEVEL 1 BLOCK DIAGRAM EXPLANATION

| | |
|---|---|
| **Module** | Microchannel Plate / Phosphor Screen DC-DC Converter |
| **Inputs** | • 13V (50mA) input power<br>• Output voltage scaling signal |
| **Outputs** | • 5.5 kV (2µA) output for Phosphor Screen<br>• 2.5kV (50µA) output for Microchannel Plate |
| **Functionality** | To scale the input power to high voltage for the microchannel plate and phosphor screen according to the programmable input |
| **Module** | Voltage / Current Monitoring Circuits |
| **Inputs** | • DC-DC converter output power<br>• -7V (8mA) analog rail |
| **Outputs** | • Voltage monitoring signal<br>• Current monitoring signal |
| **Functionality** | To provide the instrument control package with DC signals corresponding to the output voltage and current to monitor operating conditions |
| **Module** | Output Voltage Scaling Circuit |
| **Inputs** | • 0V to -5V programmable input |
| **Outputs** | • DC-DC converter output voltage scaling signal |
| **Functionality** | To linearly scale the output voltage from 0% at 0V to 100% at -5V |

Figures 3-3 through 3-5 provide further detail of the system in Level 2 block diagrams. The microchannel plate and phosphor screen operate similarly so one block diagram will be used to explain the same functions for both outputs. Figure 3-3 shows the DC-DC converter power stage, Figure 3-4 shows the voltage and current monitoring circuit, and Figure 3-5 shows the output voltage scaling circuits.

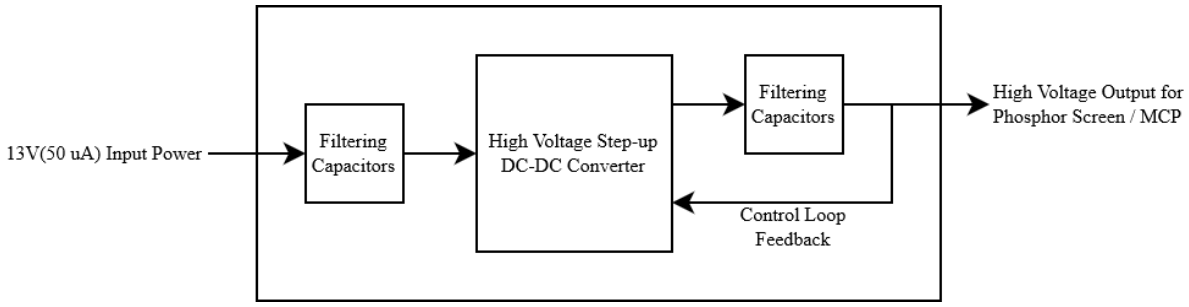


*Figure 3-3: Level 2 block diagram for the DC-DC converter (power stage)*

TABLE 3-3: LEVEL 2 BLOCK DIAGRAM EXPLANATION

| **Module** | High Voltage Step-up DC-DC Converter |
|---|---|
| **Inputs** | • 13V (50mA) input power |
| **Outputs** | • 5.5 kV (2µA) output for Phosphor Screen / 2.5kV (50µA) output for Microchannel Plate |
| **Functionality** | To scale the low input voltage to high output voltages for the phosphor screen and microchannel plate |
| **Module** | Filtering Capacitors |
| **Inputs** | • 13V (50mA) input power / High voltage output |
| **Outputs** | • Filtered input voltage / Filtered output voltage |
| **Functionality** | To reduce voltage and current ripple before entering the DC-DC converter and exiting the power supply |

The use of filtering capacitors is crucial to meeting the output voltage ripple specification. In the real world a capacitor has an equivalent series resistance between 0.1Ω and 10Ω which increases output voltage ripple. One way to minimize this effect is to place multiple capacitors in parallel to significantly reduce their total resistance.

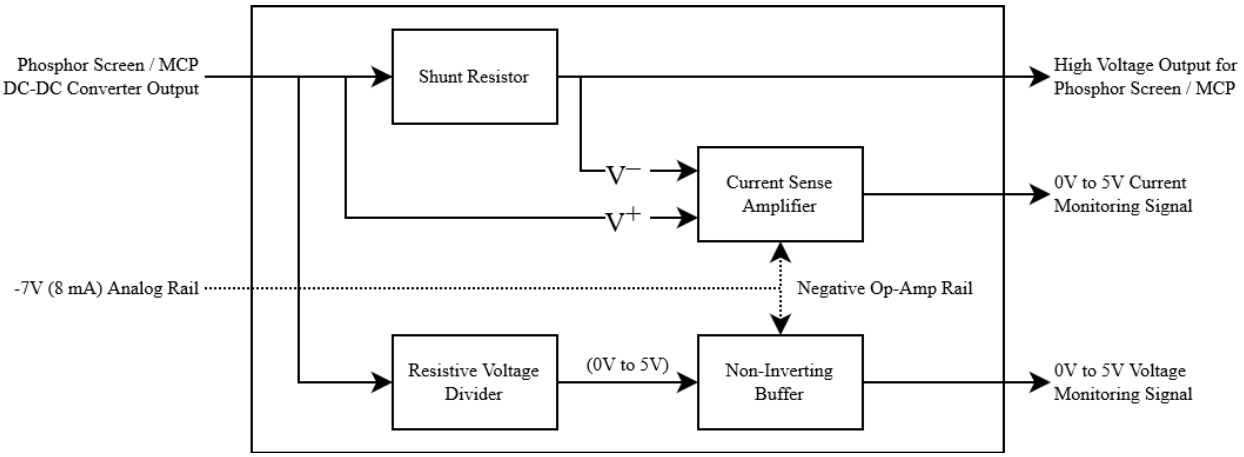


*Figure 3-4: Level 2 block diagram for the voltage and current monitoring circuits (same design for both microchannel plate and phosphor screen)*

TABLE 3-4: LEVEL 2 BLOCK DIAGRAM EXPLANATION

| **Module** | Shunt Resistor + Current Sense Amplifier |
|---|---|
| **Inputs** | • Output current (in series with load) |
| **Outputs** | • Variable DC voltage (0V to 5V) based on load current |
| **Functionality** | To sense the output current and convert it to a variable voltage |
| **Module** | Resistive Voltage Divider + Non-inverting Buffer |
| **Inputs** | • Output voltage (in parallel with load) |
| **Outputs** | • Variable DC voltage (0V to 5V) based on load voltage |
| **Functionality** | To monitor the output voltage for the instrument control package |

The easiest way to measure load current is to use a current sense amplifier with a series connected shunt resistor. This converts the load current into a differential voltage which is amplified before sending the signal back to the instrument control package. The voltage drop across the resistor scales linearly with the load current and can provide accurate measurement at low currents.

The easiest way to measure output voltage is to use a resistive voltage divider in parallel with the load that produces 5V at the output when the output voltage is at 100%. Then to prevent loading effects on the divider, a non-inverting buffer op-amp is used to send the divider voltage to the instrument control package.

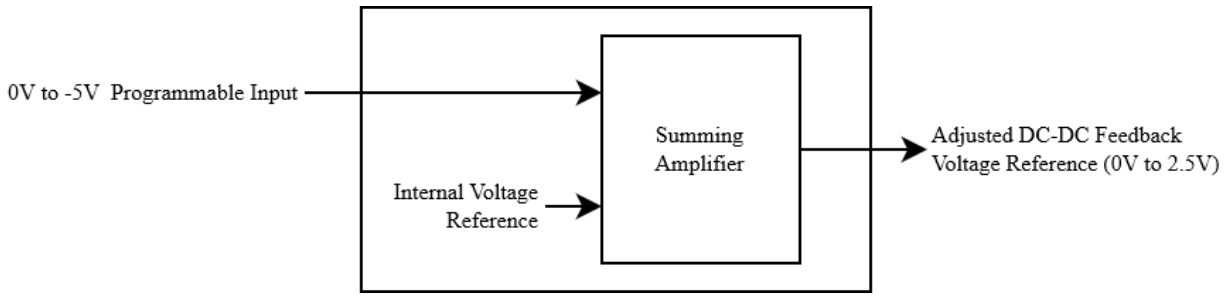


*Figure 3-5: Level 2 block diagram for the output voltage scaling circuit (same design for both the microchannel plate and phosphor screen)*

TABLE 3-5: LEVEL 2 BLOCK DIAGRAM EXPLANATION

| **Module** | Summing Amplifier |
|---|---|
| **Inputs** | • Microchannel plate / phosphor screen programmable input (0V to -5V)<br>• Internal voltage reference (5V) |
| **Outputs** | • Adjusted DC-DC converter feedback voltage reference |
| **Functionality** | To adjust the DC-DC converter's feedback reference voltage based on the programmable input signal |

One solution for the output voltage scaling circuit is to adjust the DC-DC converter's feedback voltage reference in response to the programmable input voltage. In Figure 3-5 a summing amplifier adds the 0V to -5V programmable input with an internal reference voltage and uses the difference to move the DC-DC converter's feedback voltage reference point. Ideally with the programmable input set to 0V the DC-DC converter does not operate the MOSFET switch and keeps the output voltage at 0%. This can be achieved if the summing amplifier can force the feedback node's voltage to match the DC-DC controller's internal reference. Then with the programmable input set to -5V the DC-DC converter operates under steady state conditions and the summing amplifier no longer adjusts the controller's feedback reference voltage.

Additional validation criteria were obtained from the sponsor and all technical specifications are summarized in Table 3-6. The imaging equipment operates at high frequency (over 50 GHz) and is sensitive to voltage and current fluctuations. To prevent electromagnetic interference the DC-DC converter's switching frequency is limited to 500 kHz to ensure there

are at least two orders of magnitude between the switching signal and the imaging equipment. Figure 3-6 shows an overview of the available volume for both circuit board and components. The volume specifications were provided by the Mechanical Engineering team. The available board area is small but surface mount components will be used to reduce component footprints. Unfortunately, the available height is extremely limited so transformer and inductor sizing will be the most crucial element in design equations. The shorter portion of the board lies directly between the cube satellite's wall and the imaging equipment, and the taller portion lies in front of the imaging equipment between the wall and path of incoming light. If components in either area are too tall then there will be conflicts with the imaging equipment and could render the satellite unusable.

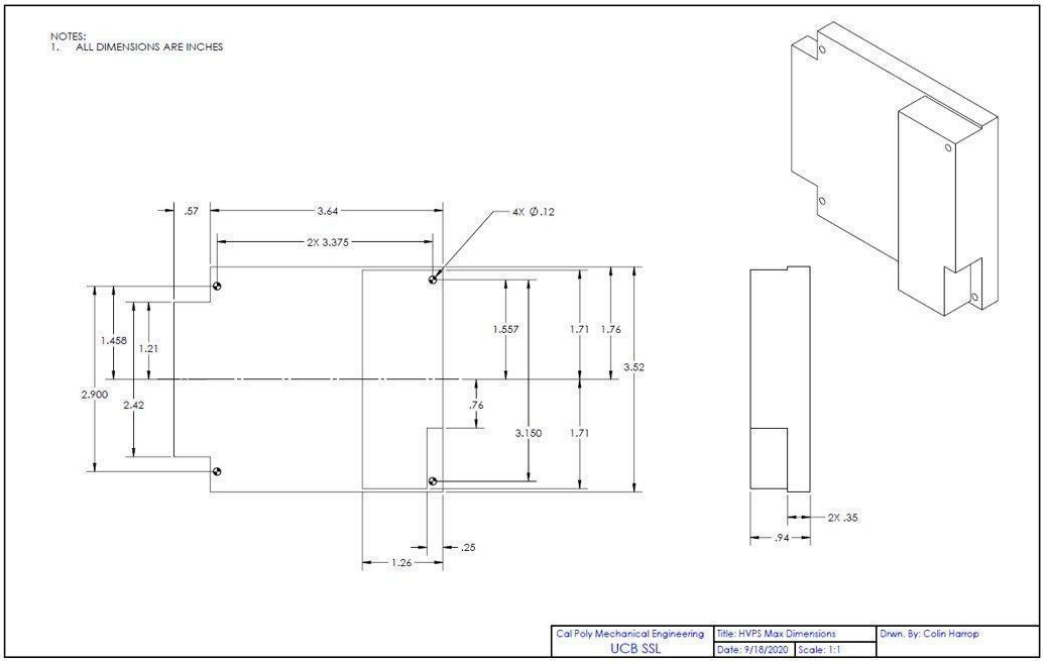


*Figure 3-6: Mechanical specifications for board area and component height*

TABLE 3-6: SUMMARY OF MUVI SATELLITE HVPS REQUIREMENTS AND SPECIFICATIONS

| Requirements | Engineering Specifications | Justification |
|---|---|---|
| 3, 4 | Power supply provides the Phosphor Screen with at least 5.5 $kV_{DC}$ up to 2uA with less than 7ppm voltage ripple (38.5 mV peak-to-peak). | The 5.5 kV source powers the Phosphor Screen. Excessive voltage ripple can damage sensitive imaging equipment. |
| 3, 4 | Power supply provides the Microchannel Plate with at least 2.5 $kV_{DC}$ and up to 50uA with less than 7ppm voltage ripple (17.5 mV peak-to-peak). | The 2.5 kV source powers the Microchannel Plate. Excessive voltage ripple can damage sensitive imaging equipment. |
| 5 | Output voltage for Phosphor Screen and Microchannel Plate scales linearly from 0% to 100% based on 0V to -5V input signal. Maximum output voltage occurs at -5V input. | Scalable output voltage allows safer testing conditions in UC Berkeley's vacuum chamber. |
| 4, 8 | Power supply provides output voltage, output current, and temperature monitoring to the instrument control package (ICP) within ±2% accuracy. | Voltage, current, and temperature information allows the customer to monitor operation while testing in vacuum and in orbit. |
| 2 | Positive input power source provides 13 $V_{DC}$ (±5%) and up to 50 mA. Negative input power source provides -7 $V_{DC}$ (±5%) and up to 8 mA. | Instrument Control Package (ICP) provides input power sources (designed by UC Berkeley for ICON mission). The positive voltage source powers the DC-DC converter and the negative voltage source powers the negative analog voltage rail. |
| 7 | All silicon-based components must be radiation hardened to withstand 20kRad or more over a 2-year lifespan | Non-radiation hardened components are easily damaged in the ionosphere which causes premature system failure |
| 1 | The printed circuit board area does not exceed 3.64" width x 3.52" length. The component height does not exceed 0.35" directly underneath the imager and 0.91" in front of the imager (see Colin Harrop's CAD drawing in Figure 3-6) | Cube satellite size specifications restrict the circuit board mounting area. Circuit board mounts directly underneath the imager and constrains component height. Part of the circuit board extends out from under the imager and components there cannot block the light input area. |
| 6, 8 | All components operate between 0°C and 30°C in vacuum. This applies to testing and space environments | Mounting the imager directly above the circuit board risks heat absorption, damage, and/or distortion to the imaging equipment. |
| 8 | The connectors used to link the HVPS to the MCP and phosphor screen must exceed the max operating voltage and current by at least 50% | Overrating the connectors ensures the components experience little stress during operation |

**List of Marketing Requirements**

1. Small enough to mount inside a cube satellite
2. Able to operate from a low power input source
3. Produces high voltage for imaging device
4. Output voltage has minimal noise
5. Output voltage scales linearly for testing purposes
6. Does not generate excessive heat
7. Silicon components must withstand harsh space environment
8. Provides output and temperature monitoring

# Chapter 4 – Design

The first step in designing a DC-DC converter is selecting a suitable topology. The available topologies for this project are a push-pull stage cascaded to voltage multiplier stage, a single flyback stage, and boost stage cascaded to flyback stage. Each topology has strengths and weaknesses that will help determine if it is suitable based on the design requirements. Table 4-1 displays the differences between the available topologies.

TABLE 4-1: SUMMARY OF AVAILABLE STEP-UP DC-DC CONVERTER TOPOLOGIES

| Topology | Strengths | Weaknesses |
|---|---|---|
| Push-Pull & Multiplier | ● Low input and output ripple<br>● Easy to simulate | ● Many stages / high complexity<br>● Limited frequency range<br>● High cost for multiplier<br>● Slow response time due to multiplier propagation delay |
| Flyback | ● Simple design / low complexity<br>● Lower cost than other topologies<br>● Higher efficiency than a 2-stage approach | ● Requires a transformer with high turns ratio (30 or more)<br>● High input and output noise<br>● Requires additional output filtering |
| Boost & Flyback | ● Higher input voltage allows the use of a transformer with lower turns ratio (10 or greater)<br>● Boost reduces input noise<br>● Increases design flexibility<br>● Better voltage regulation and accuracy with 2 controllers | ● Lower efficiency than a single stage design<br>● Requires 2 controllers<br>● Requires additional output filtering |

Each topology listed in Table 4-1 is a suitable candidate for this high voltage DC-DC converter. The next step to better understand which option is best for this application is to look at design equations to determine which converter has the best component values and ratings. Each topology requires different component values and applies stresses on each component differently. This affects complexity, price, and feasibility of a particular component's use. The design requirements from Chapter 3 state the input voltage is 13V and the output voltage is

2.5kV for the microchannel plate and 5.5kV for the phosphor screen. These values are then plugged into the various design equations for each topology to determine the important design criteria. The most important values to consider for this project are duty cycle, inductor size, transformer turns ratio, MOSFET drain-source voltage, and diode reverse voltage.

The first topology under review is the push-pull converter cascaded to a voltage multiplier. A push-pull converter uses two switches that each occupy half of the switching period which limits the duty cycle to 50% maximum. A duty cycle of 25% is chosen for simplicity and flexibility for further optimization. If a ten stage Cockcroft-Walton voltage multiplier is used, then only $250V_{AC}$ output is required for the microchannel plate and $550V_{AC}$ for the phosphor screen. Equation 4-1 calculates the required transformer turns ratio to achieve $550V_{AC}$ for the phosphor screen (worst-case scenario).

$$n = \frac{\bar{V}_0}{2\bar{V}_{IN}D} = \frac{550\ V_{pk-pk}}{2\ \cdot\ 13\ V\ \cdot\ 0.25} = 1:85\ turns \qquad (4 - 1)$$

At 25% duty cycle the turns ratio is 1:85 which is large and requires a transformer that does not fit in the available area. Performing another iteration at 45% duty cycle reduces the required turns ratio to 1:47 which is still too high. After one design equation the push-pull converter is eliminated from the list of potential topologies.

The next topology under review is the flyback converter. Flyback converters use only one switch and can have a duty cycle between 0% and 100%. A conservative duty cycle, which accounts for limitations in switching speed, is 80%. Equation 4-2 calculates the required turns ratio to be 1:106 for the phosphor screen which is even higher than the push-pull converter.

$$n = \frac{\bar{V}_0\ (1\ -\ D)}{\bar{V}_{IN}D} = \frac{5.5\ kV\ \cdot\ (1\ -\ 0.8)}{13\ V\ \cdot\ 0.8} = 1:106\ turns \qquad (4 - 2)$$

One way to decrease the required turns ratio is to increase the input voltage being fed to the flyback stage. If the input voltage is raised to 92V or more, then the new turns ratio is 1:15. This is a much more reasonable value. To see if the same 1:15 turns ratio works for the microchannel plate, it is plugged back into equation 4-2 and rearranged to solve for Vin. Equation 4-3 shows the result. According to equation 4-3 the converter requires 41.7V or more to produce 2.5kV on the output.

$$\bar{V}_0 = \frac{\bar{V}_0\,(1\ -\ D)}{n\ \cdot\ D} = \frac{2.5\ kV\ \cdot\ (1\ -\ 0.8)}{15\ \cdot\ 0.8} = 41.7\ V \tag{4 - 3}$$

This is where the boost-flyback converter solves all of the issues of the previous two topologies. The first stage is a boost converter that takes the 13V input and increases it to 92V for the phosphor screen and 42V for the microchannel plate before sending it to the flyback transformer. Another benefit of this approach arises from the boost converter inductor connected to the input. The inductor reduces current ripple at the DC input more than the flyback stage alone. Equations 4-4 through 4-7 are to characterize the phosphor screen boost converter. D is duty cycle, $L_C$ is critical inductance, $I_{SW}$ is average switch current, and $V_{diode}$ and $V_{SWmax}$ are maximum diode and switch voltages.

$$D_{boost} = 1 - \frac{\bar{V}_{IN}}{\bar{V}_0} = 1 - \frac{13\ V}{92\ V} = 85.87\% \tag{4 - 4}$$

$$L_C = \frac{D\ \cdot\ (1-D)^2\ \cdot\ \bar{V}_0}{2\ \cdot\ f_S\ \cdot\ \bar{I}_{0min}} = \frac{0.859\ \cdot\ (1-0.859)^2\ \cdot\ 92\ V}{2\ \cdot\ 500\ kHz\ \cdot\ 10\ mA} = 157.2\ \mu H \tag{4 - 5}$$

$$\bar{I}_{SW} = \bar{I}_L D = 10\ mA \cdot 0.859 = 8.59\ mA \tag{4 - 6}$$

$$\hat{V}_{diode} = \hat{V}_{SWmax} = \bar{V}_0 + \frac{\Delta\bar{V}_0}{2} = 92\ V + \frac{1\ V}{2} = 92.5\ V \tag{4 - 7}$$

All the boost equations lead to reasonable component values and tolerances. The next step is to characterize the flyback stage using 92V as the input voltage and 1:15 transformer turns ratio. Equations 4-8 through 4-11 are for the phosphor screen flyback converter.

$$D_{flyback} = \frac{\bar{V}_0}{\bar{V}_{IN} \cdot \frac{N_2}{N_1} + \bar{V}_0} = \frac{5.5\ kV}{92\ V \cdot \frac{15}{1} + 5.5\ kV} = 79.9\% \quad (4 - 8)$$

$$\hat{V}_{SWmax} = \bar{V}_{IN} + (\bar{V}_0 \frac{N_1}{N_2}) = 92 + (5.5\ kV \cdot \frac{1}{15}) = 458.66\ V \quad (4 - 9)$$

$$\hat{V}_{RRM} = \bar{V}_0 + \bar{V}_{IN} \frac{N_2}{N_1} = 5.5\ kV + (92\ V \cdot \frac{15}{1}) = 6.88\ kV \quad (4 - 10)$$

$$C_O = \frac{D \cdot \bar{I}_0}{f_{SW} \cdot \Delta\bar{V}_0} = \frac{0.799 \cdot 2\ \mu A}{500\ kHz \cdot 34\ mV} = 94\ pF \quad (4 - 11)$$

At 80% duty cycle and 1:15 turns ratio, the phosphor screen flyback converter requires high voltage ratings which will limit the selection of MOSFETs. The requirement to be radiation hardened and have a high voltage rating greatly decreases the number of viable and commercially available options. Equations 4-12 through 4-15 characterize the microchannel plate's flyback converter.

$$D_{flyback} = \frac{\bar{V}_0}{\bar{V}_{IN} \frac{N_2}{N_1} + \bar{V}_0} = \frac{2.5\ kV}{92 \cdot \frac{15}{1} + 2.5\ kV} = 79.9\% \quad (4 - 12)$$

$$\hat{V}_{SWmax} = \bar{V}_{IN} + (\bar{V}_0 \frac{N_1}{N_2}) = 42 + (2.5\ kV \cdot \frac{1}{15}) = 208.66\ V \quad (4 - 13)$$

$$\hat{V}_{RRM} = \bar{V}_0 + \bar{V}_{IN} \frac{N_2}{N_1} = 2.5\ kV + (42\ V \cdot \frac{15}{1}) = 3.13\ kV \quad (4 - 14)$$

$$C_O = \frac{D \cdot \bar{I}_0}{f_{SW} \cdot \Delta\bar{V}_0} = \frac{0.799 \cdot 50\ \mu A}{500\ kHz \cdot 18\ mV} = 4.44\ nF \quad (4 - 15)$$

Once again, the voltage ratings for the MOSFET and diode are high but remain lower than the phosphor screen. To make part procurement easier, both flyback converters will use the same MOSFET and diode.

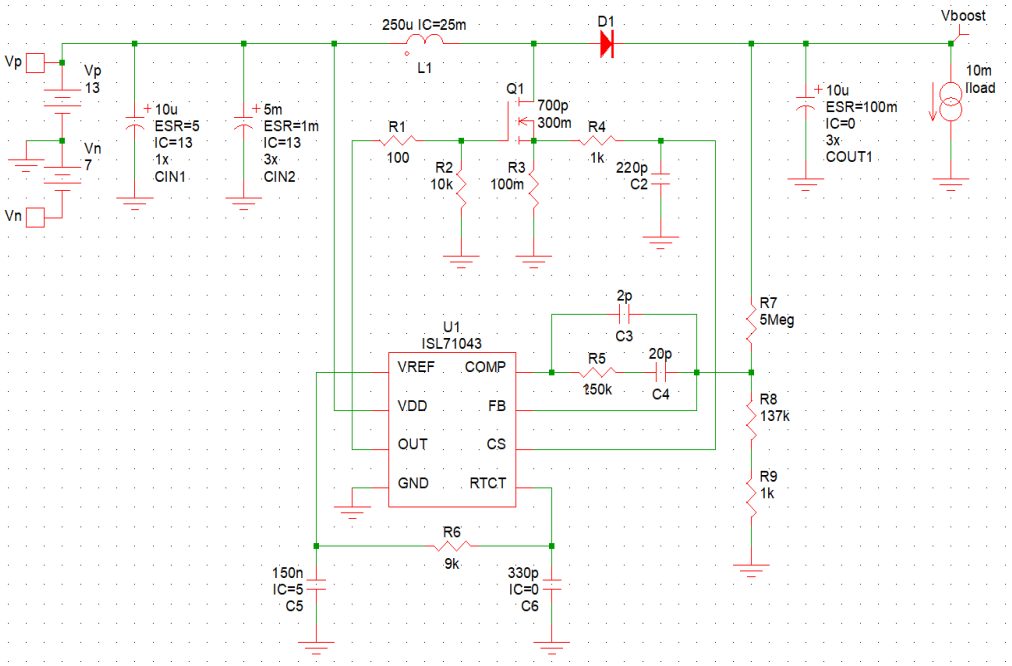


*Figure 4-1: Boost converter for the phosphor screen using the ISL71043 controller. Input = 13V and output = 92V.*

The design can be tested using computer-based circuit simulators like LTspice, Pspice, or Simplis. The first step is to select a controller IC for the DC-DC converters. One convenience with boost and flyback converters is that they can use the same PWM low-side switch controller, so research time is cut in half. All silicon-based components must be radiation hardened to withstand at least 10 kRad over a 5-year period which severely limits the list of commercially available components. The ISL71047 low-side switch PWM controller by Renesas fits all of the criteria and has a Simplis simulation model. Figure 4-1 shows the boost converter for the phosphor screen and Figure 4-2 shows the simulation results for the microchannel plate (left) and phosphor screen (right).

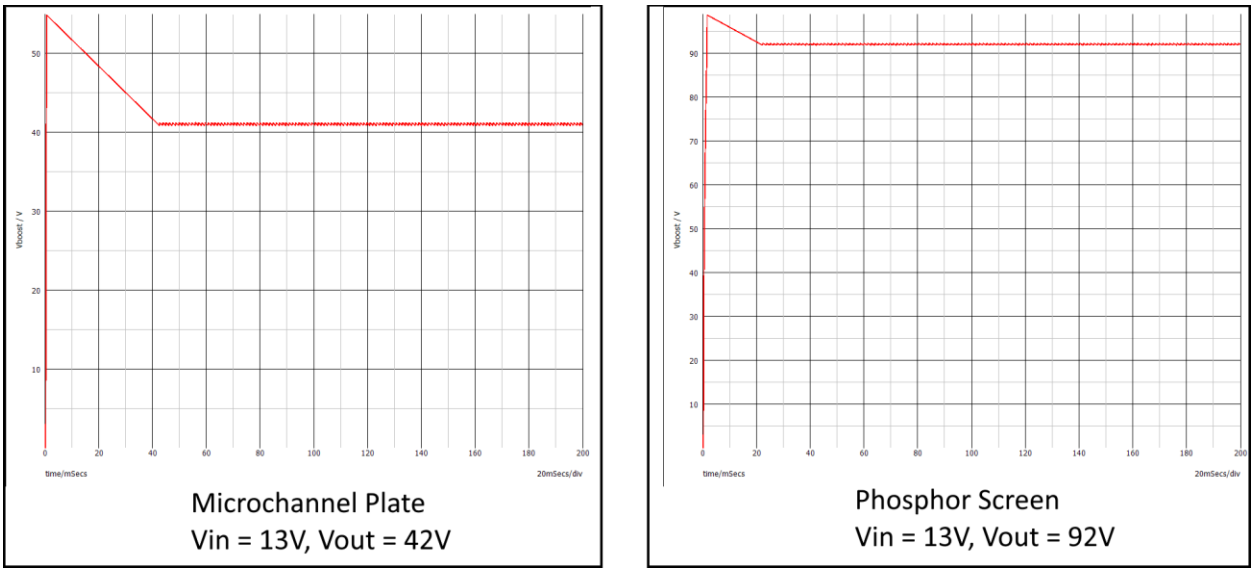


*Figure 4-2: Boost converter simulation results for the microchannel plate and phosphor screen*

As seen in Figure 4-2 the boost converter can achieve the required output voltages for the microchannel plate (42V) and phosphor screen (92V). The only difference between the two converters is the feedback voltage divider ratio and error compensation network (resistors and capacitors connected to the COMP pin). Figure 4-3 shows the schematic of the phosphor screen flyback converter using the same ISL71043 controller.

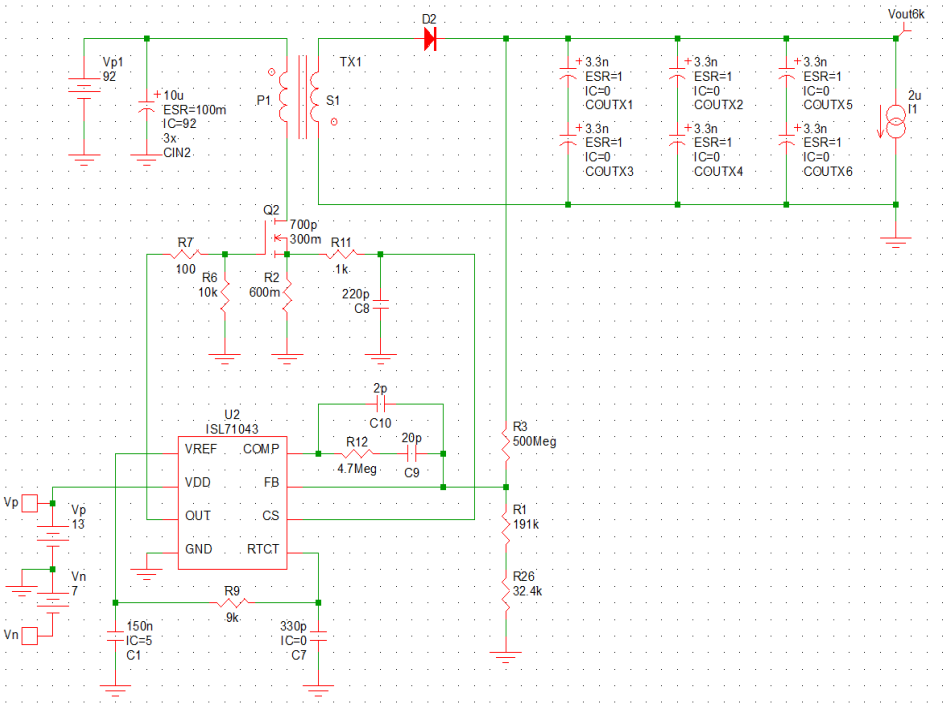

*Figure 4-3: Schematic of the Phosphor Screen's flyback converter using 92V for the input*

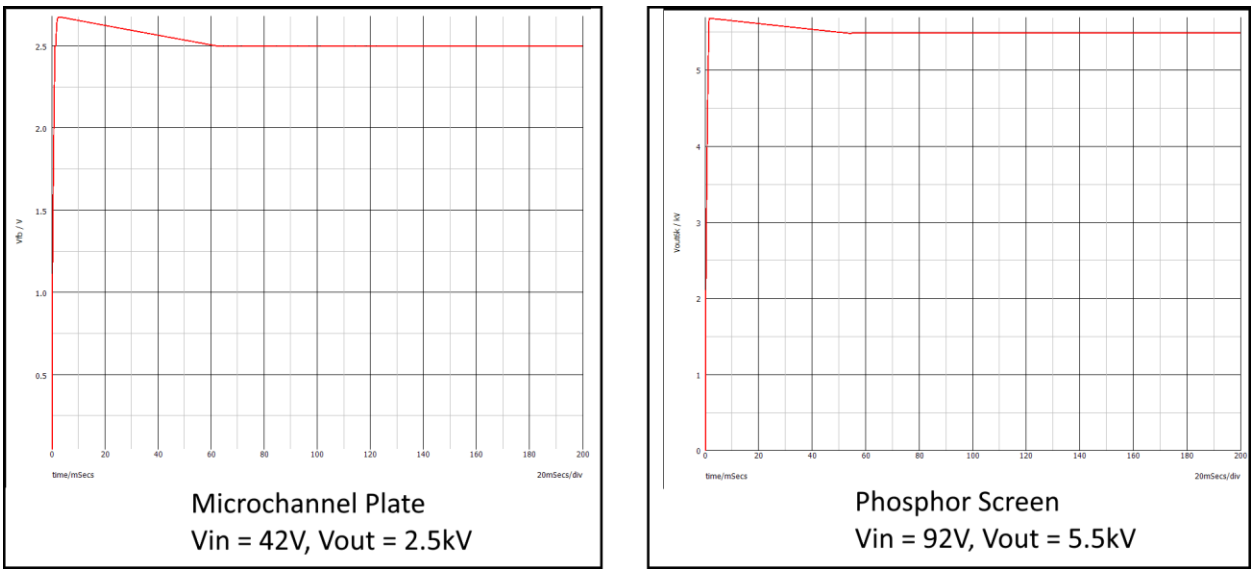


*Figure 4-4: Simulation results for the flyback converter (note the y-axis is in kV)*

Once again, the simulation can achieve the desired output voltages for the microchannel plate and phosphor screen. The output remained steady at 2.5kV with 16mV of ripple for the microchannel plate and 5.5kV with 34mV of ripple for the phosphor screen. The transient period does show some overshoot at the beginning due to the compensation network which will be optimized during hardware testing. After the initial overshoot, the output voltage settles at the expected value and continues in steady-state operation. Figure 4-5 is the schematic for the cascaded boost and flyback converter and 4-6 are the simulation results.

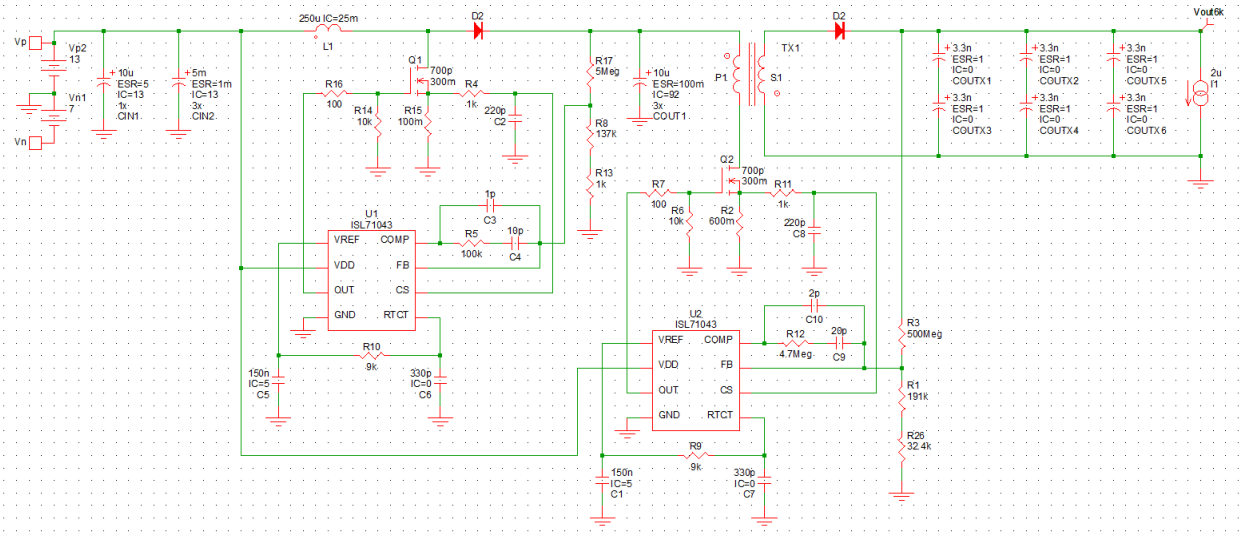


*Figure 4-5: Schematic for the boost cascaded to flyback converter*

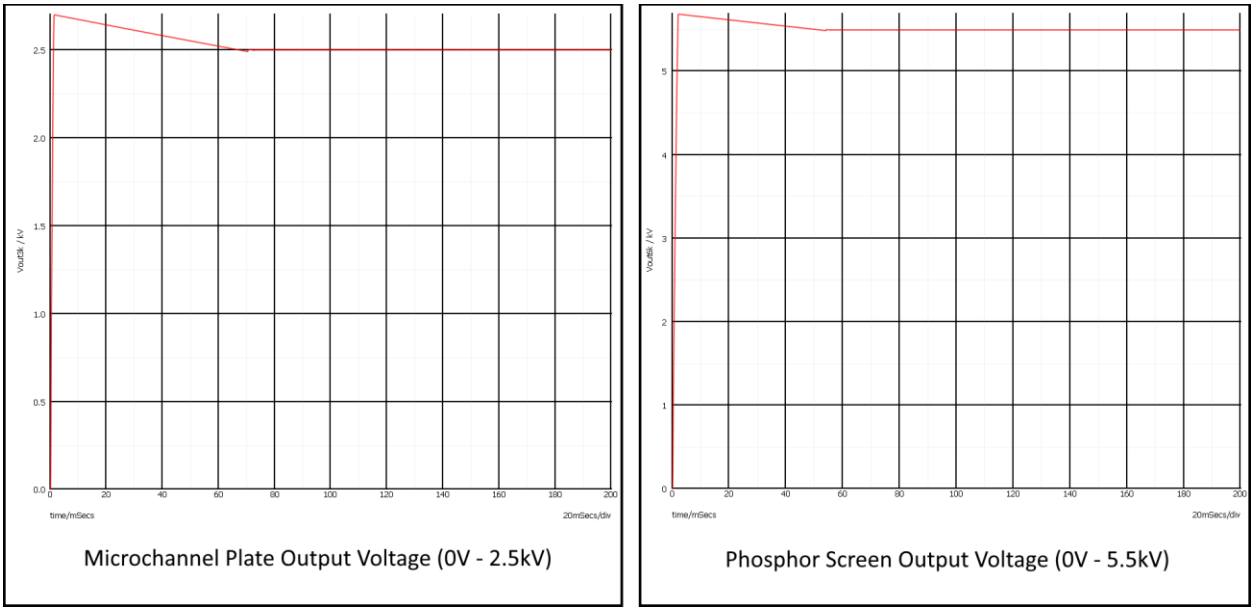


*Figure 4-6: Simulation results for the boost cascaded to flyback (note the y-axis is in kV)*

The simulation results in Figure 4-6 show that the microchannel plate and phosphor screen can achieve stable output voltages as expected. The microchannel plate sustains 2.5kV with 16mV of ripple and the phosphor screen sustains 5.5kV with 34mV of ripple.

Now that the power stage design is finished, the focus shifts to designing the programmable input, voltage monitoring, and current monitoring circuits. Figure 4-7 is the schematic for a prototype programmable input. It works by adjusting the base voltage of the

feedback voltage divider used by the controller to regulate the output voltage. When the feedback pin of the controller sees 2.5V or more it stops the MOSFET from switching and waits until the voltage lowers before switching again. By raising and lowering the base voltage of the voltage divider we can trick the controller into thinking it is in steady state at different output voltages. If a low output voltage is desired, then the base of the feedback voltage divider is raised close to 2.5V and only a small amount of output voltage is required to raise the feedback to 2.5V. When a large output voltage is desired then the base of the feedback voltage divider is lowered close to ground and a large amount of output voltage is required to raise the feedback to 2.5V.

The solution consists of an inverting summing op-amp cascaded into another inverting op-amp with a gain of 0.5. The summing op-amp takes a 5V reference and the negative programmable input voltage and outputs an inverted difference between the two voltages. When the programmable input is 0V the summing op-amp outputs -5V and when the programmable input is -5V the op-amp outputs 0V. The ISL71047 controller conveniently provides the required 5V reference. Then the second inverting op-amp divides the summing op-amp's output by two to give us 0V - 2.5V at the base of the flyback voltage divider. The design provides high resolution that is limited by the programmable input signal's step size.

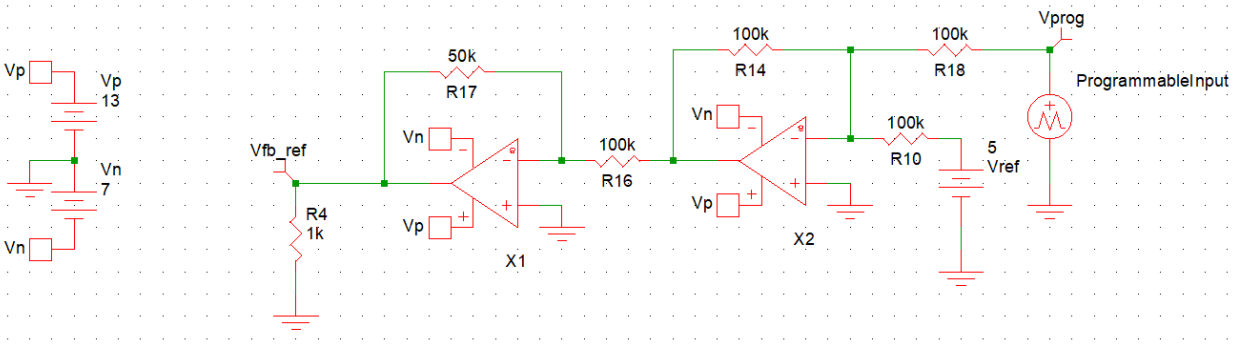


*Figure 4-7: Programmable input circuit for controlling flyback output voltage. The same design is used for the microchannel plate and phosphor screen*

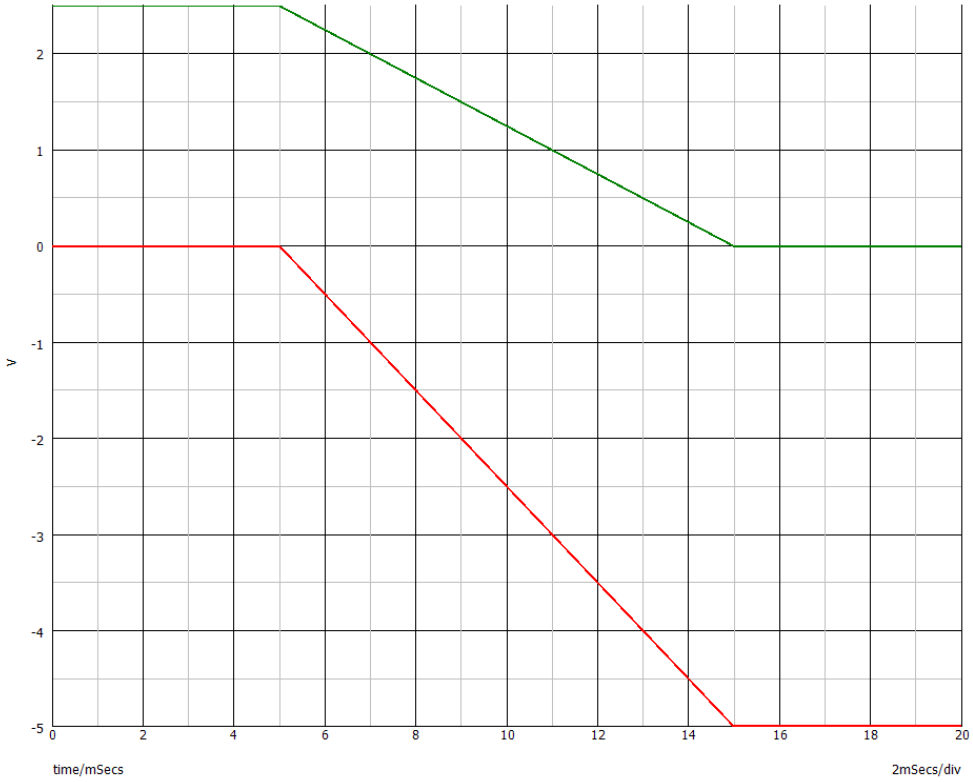


*Figure 4-8: Programmable input and base feedback voltage from 0V to -5V*

The simulation results are shown in Figure 4-8 for the programmable input system where the bottom red line is the programmable input (0V to -5V) and the top green line is the base voltage of the voltage divider (2.5V to 0V). The system behaves as expected and provides a linear relationship between the programmable input and the flyback voltage divider base voltage.

Figure 4-9 shows the schematic for the prototype voltage monitoring system. It was taken from ICON's system and adapted for higher switching frequency. It uses a voltage divider and non-inverting buffer with compensation network to measure a small portion of the output voltage. The voltage monitoring system reports 5V back to the instrument control package when the output voltage is within ±1% of its maximum. The same system is used for the microchannel plate and phosphor screen but with slightly different voltage divider ratios. The negative feedback resistor (R24) and capacitor (C11) form a compensation network to attenuate the op-amp's natural tendency to amplify signals near the switching frequency.

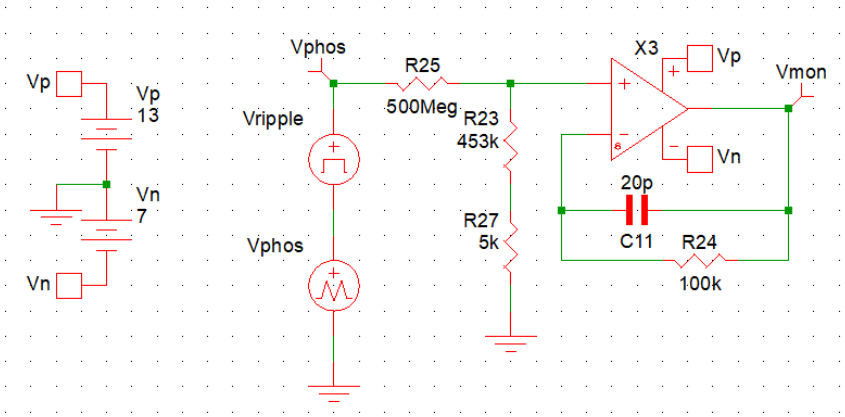


*Figure 4-9: Schematic for the voltage monitoring system*

The simulation results in Figure 4-10 show a linear relationship between the voltage monitoring output and the flyback output voltage. The voltage monitoring system accurately measures the flyback output voltage and scales it down between 0V (0%) and 5V (100%). The steady flyback DC output and the negative feedback compensation network provide a stable and near ripple-free monitoring signal.

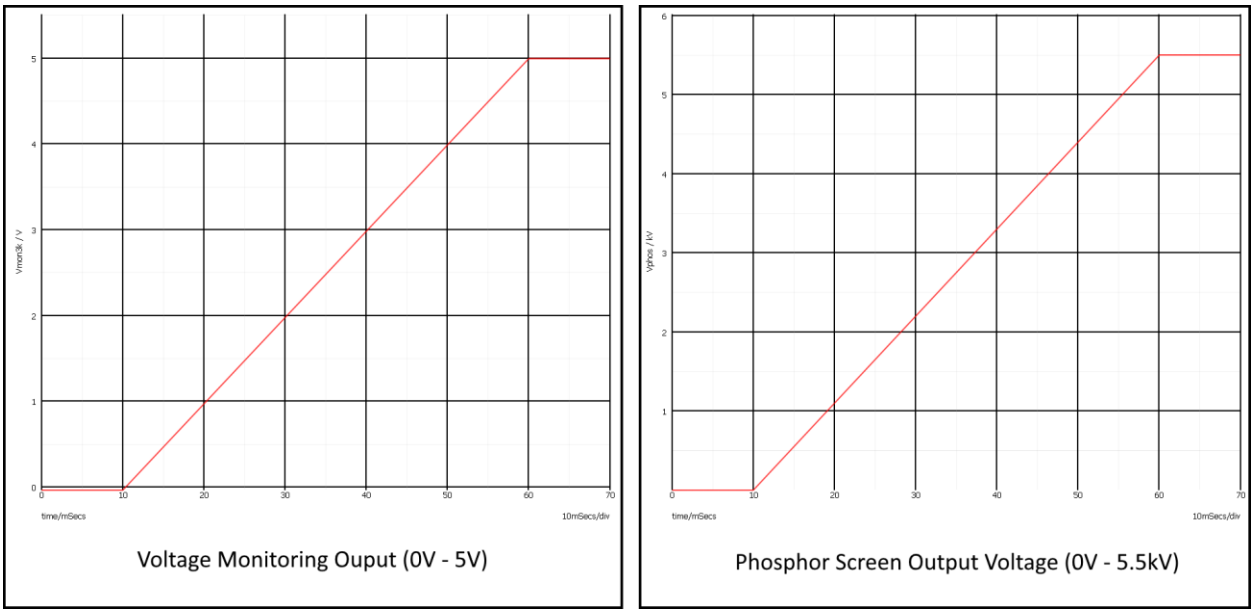


*Figure 4-10: Simulation results for voltage monitoring system*

Lastly, the current monitoring circuit samples the load current through a shunt resistor. Then it amplifies the sensed voltage to a level the instrument control package can read. At no

load current, the current monitoring circuit outputs 0V. At full load current the circuit outputs 5V. The shunt resistor is scaled such that the maximum load current produces a 1V drop across the resistor. For the microchannel plate, the shunt resistance is 16.7kΩ (up to 60µA) and the phosphor screen shunt resistance is 499kΩ (up to 2µA). The values for maximum load current were chosen based on the absolute maximum current ratings for each load. The microchannel plate can fluctuate above 50 µA if a lot of light hits the lens; however, the phosphor screen has an absolute maximum rating of 2 µA and is very sensitive to current fluctuation. Figure 4-11 shows the schematic for the current sense amplifier using the RH6105 IC from Analog Devices. RH6105 is the radiation hardened version of the LT6105 current sense amplifier.

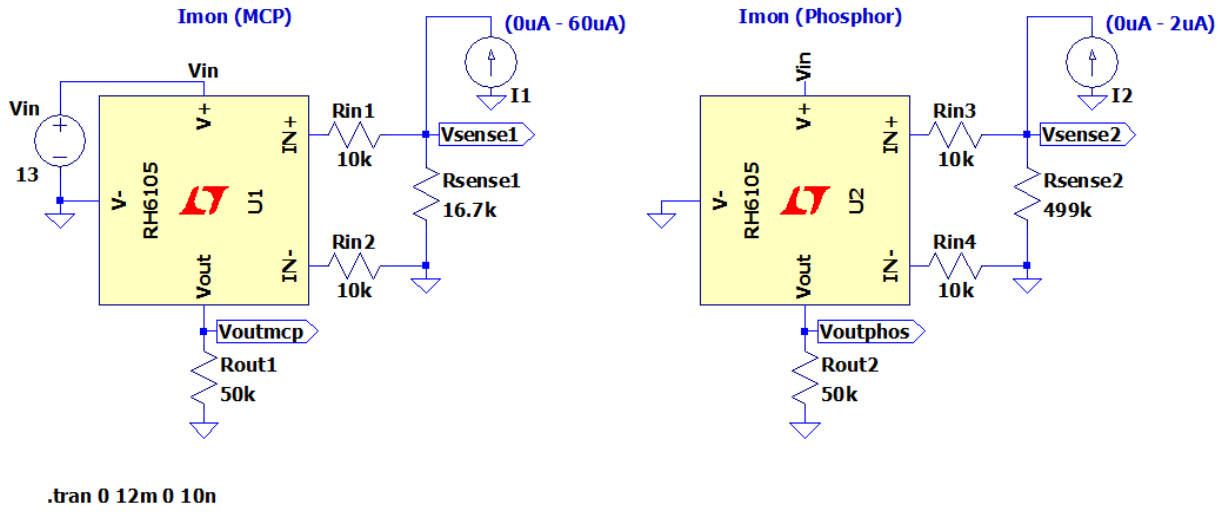


*Figure 4-11: Schematic for the current monitor system for both the microchannel plate (left) and phosphor screen (right)*

The output voltage from the RH6105 depends on the resistor ratio formed by the IN+/-, resistors, $R_{OUT}$ resistor, and voltage across the $R_{SENSE}$ resistor. With $R_{IN}$ = 10kΩ and $R_{OUT}$ = 50kΩ the output voltage is five times greater than the voltage across the sense resistor. At maximum current, the sense resistor's voltage drop is 1V so Vout should report 5V. At no current Vout should report 0V. The load currents were swept linearly, and the results are shown in Figure 4-12.

As expected, the current sense amplifier linearly scales the output voltage based on the load current. The imaging equipment is sensitive to changes in current, so the current monitoring system is crucial to controlling how much light is allowed into the microchannel plate at any given time. Accuracy will be closely measured during prototype testing.

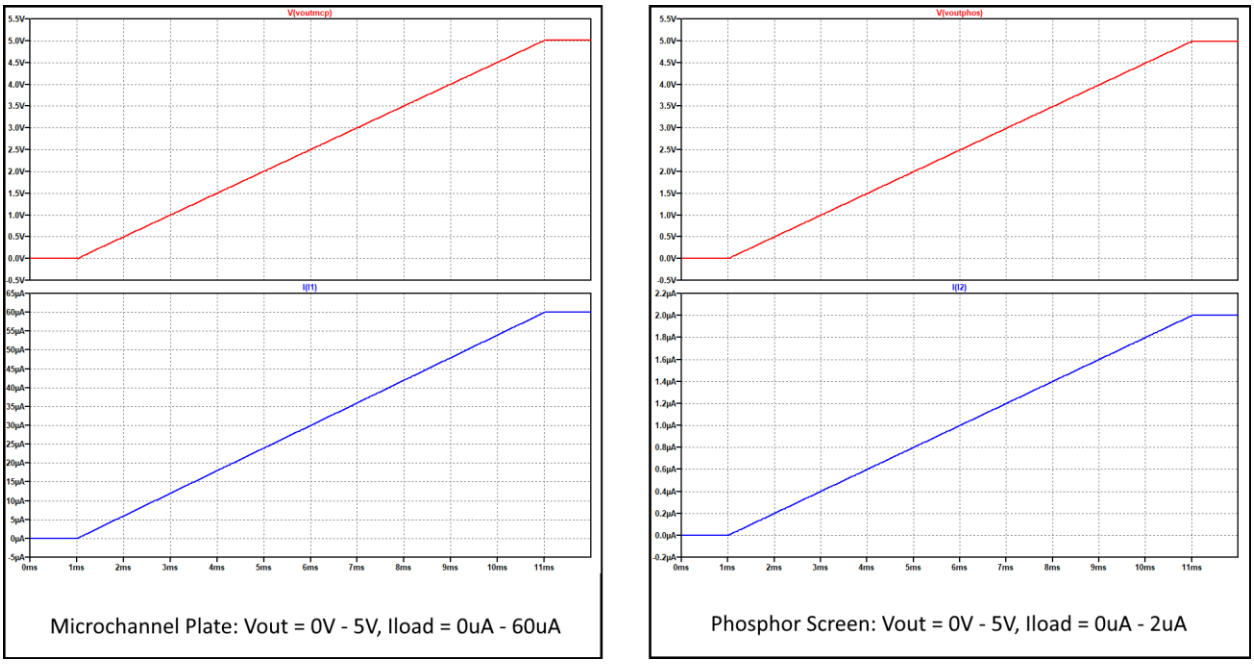


*Figure 4-12: Simulation results for the microchannel plate between 0µA - 60µA load and phosphor screen between 0µA - 2µA. $V_{OUT}$ is displayed in the top graph and $I_{LOAD}$ is displayed in the bottom graph.*

Each module in the block diagram is now designed and ready for simulation as a complete system. The entire boost-flyback schematic for the microchannel plate is pictured in Figure 4-13 and for the phosphor screen in Figure 4-15. The simulation results are pictured for the microchannel plate in Figure 4-14 and for the phosphor screen in Figure 4-16. In both simulations the programmable input is varied using a PWL voltage source and stepped in -1V increments to show how the output voltage scales linearly with programmable input voltage.

Based on the simulation results this circuit is a success and a viable solution for this application. Figure 4-14 shows the programmable input lowering by -1V steps and the output voltage increasing in approximately 1.1kV steps. Figure 4-16 shows the programmable input

voltage lowering in -1V steps and the output voltage increasing in approximately 500V steps. The input and output relationship is linear with respect to each other for both the microchannel plate and phosphor screen circuits. With the design validated through simulation, the next step is to select the remaining components, design the circuit board, assemble, and test the design.

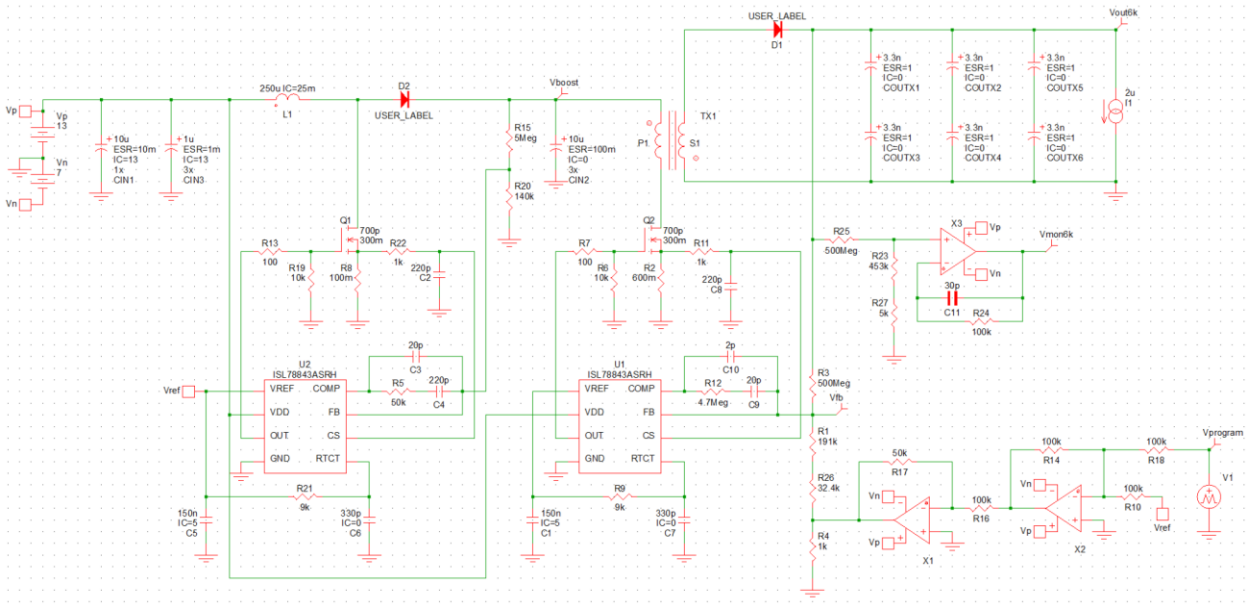


*Figure 4-13: Phosphor screen schematic with voltage monitoring and programmable input*

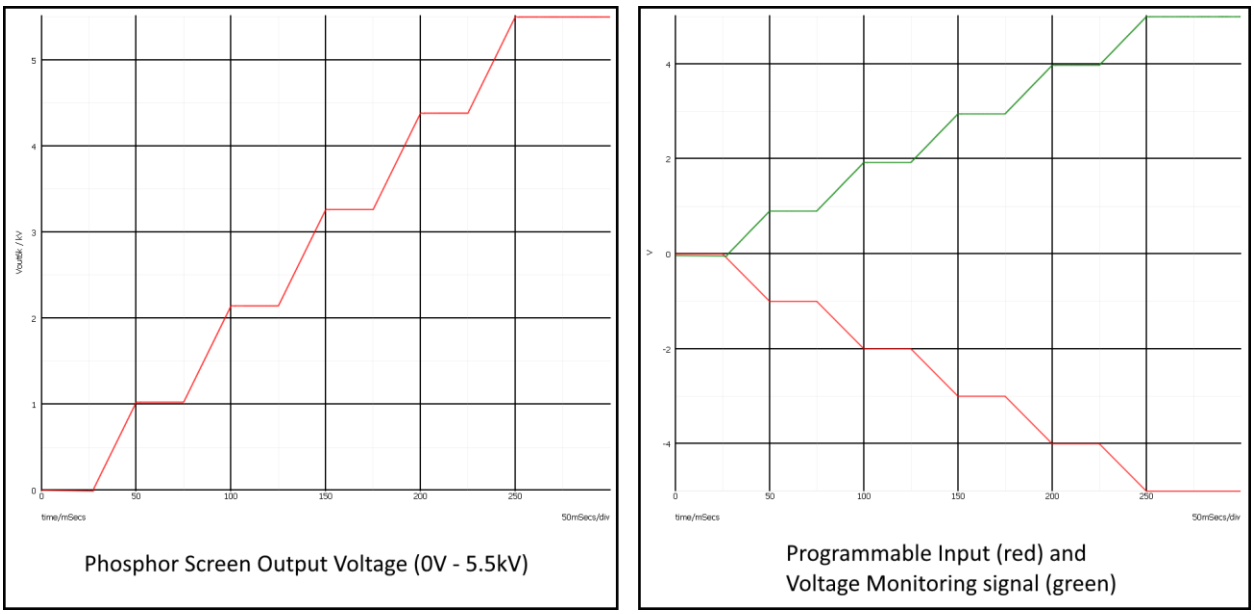


*Figure 4-14: Phosphor screen simulation results. Output voltage is shown on the left and the programmable input and output monitoring voltage is shown on the right.*

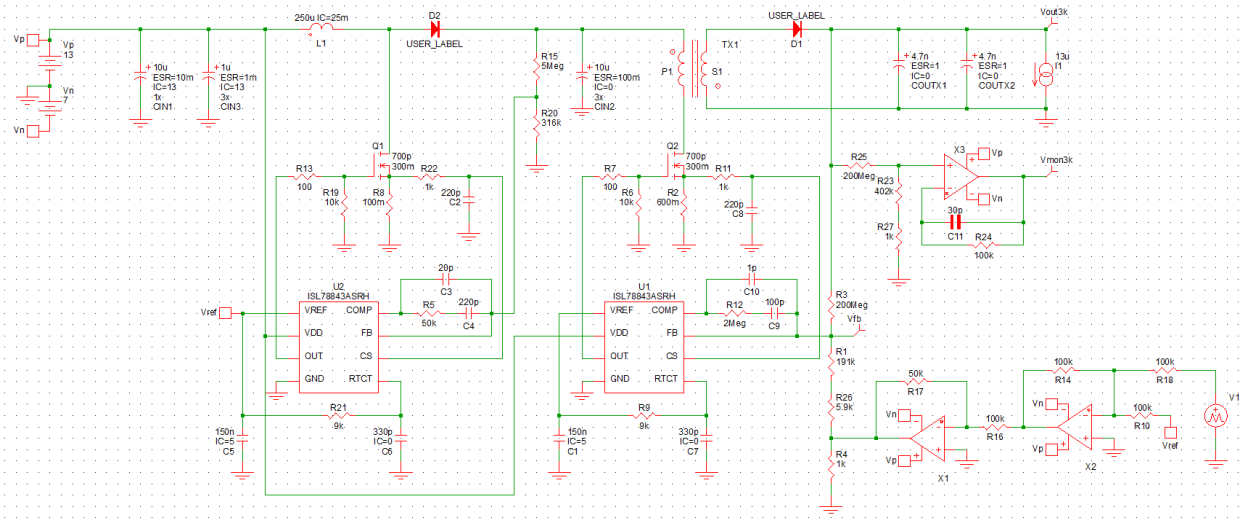


*Figure 4-15: Microchannel plate schematic with voltage monitoring and programmable input*

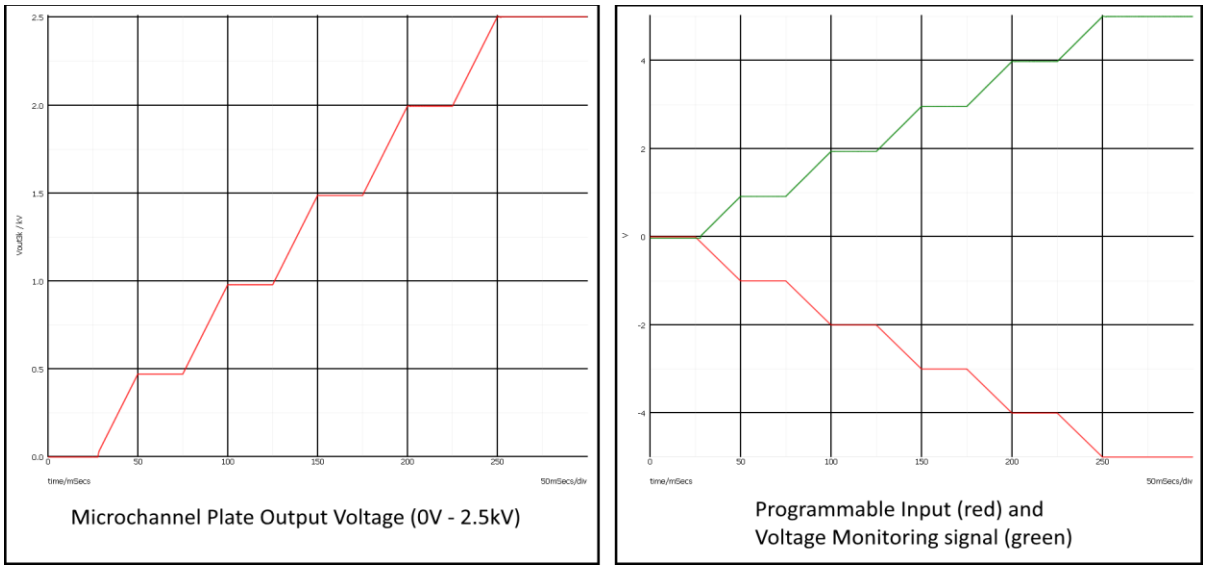


*Figure 4-16: Microchannel plate simulation results. Output voltage is shown on the left and the programmable input and output monitoring voltage is shown on the right.*

# Chapter 5 – Hardware and Test Results

After the completion of the circuit design and the verification of its functionality in simulation, component selection begins. Due to the size constraints placed on the DC-DC converter, most of the final components are selected to have a surface mount package. The larger through hole components include MOSFETs, diodes, and capacitors. These are all contained in the power path where most of the current flows. Extra care is given during component selection to ensure the integrated circuits, MOSFETs, and diodes can withstand the harsh, radiation filled environment of space. The final bill of materials is shown in Table 5-1.

TABLE 5-1: FINAL MUVI BILL OF MATERIALS

| Count | Reference Designator | Value | Description | Size | Tolerance | Part Number | Manufacturer | Per Unit Cost [$] | Per Board Cost [$] |
|---|---|---|---|---|---|---|---|---|---|
| 4 | U1, U4, U5, U8 | ISL71043MBZ | Rad Hard Boost/Flyback PWM Controller | SOIC-8 | -- | ISL70143MBZ | Renesas | $290.37 | $1,161.48 |
| 2 | U3, U7 | RH6105 | Rad Hard Current Sense Amplifier | MSOP-8 | -- | RH6105 | Analog Devices | $397.00 | $794.00 |
| 2 | U2, U6 | OPA4277-SP | Rad Hard Quad Op-Amp | CFP-14 | -- | OPA4277-SP | Texas Instruments | $950.40 | $1,900.80 |
| 4 | M1, M2, M3, M4 | IRHM7460SE | Rad Hard NMOS, 500Vds | TO-254AA | -- | IRHM7460SE | International Rectifier | | |
| 2 | D1, D3 | JAN1N5614US | Rad Hard Diode, 200Vbr (Boost) | Axial | -- | JAN1N5614US | Microsemi | $12.86 | $25.72 |
| 2 | D2, D4 | JANTX1N6526 | Rad Hard Diode, 7500Vbr (Flyback) | Axial | -- | JANTX1N6526 | doEEEt | $542.90 | $1,085.80 |
| 2 | D5, D6 | JANTX1N5618 | Transformer Snubber Diodes, 600Vbr | Axial | -- | JANTX1N5618 | SemTech | $310.10 | $620.20 |
| 1 | R21 | 11029759-00 | Rad Hard Thermistor | Axial | -- | 11029759-00 | Measurement Specialties | $237.14 | $237.14 |
| 2 | T1, T2 | -- | 1:15 Step-up Transformer | RM5 / RM6 | -- | -- | -- | -- | -- |
| 2 | L1, L2 | 250 µH | Boost Inductor | 4.5mm x 4.5mm x 3mm | 25% | 744235251 | Würth Electronic | $1.43 | $2.86 |
| 2 | R9, R28 | 500 MΩ | Phos Vmon and flyback voltage divider | 2010 | 0.5% | HVCB2010DDC500M | Stackpole Electronics | $9.25 | $18.50 |
| 2 | R43, R57 | 200 MΩ | MCP Vmon and flyback voltage divider | 2512 | 1% | HVCB2512FDD200M | Stackpole Electronics | $7.59 | $15.18 |
| 3 | R15, R25, R45 | 5.1 MΩ | Phos flyback compensation, Boost divider | 0805 | 1% | RC0805FR-075M1L | Yageo | $0.13 | $0.39 |
| 1 | R53 | 2 MΩ | MCP flyback compensation | 0805 | 1% | ERJ-6ENF2004V | Panasonic | $0.10 | $0.10 |
| 3 | R11, R72, R73 | 499 kΩ | MCP current sense Rout, Phos Rsense, Phos Rout | 0805 | 0.1% | 6AEB4993V | Panasonic | $0.36 | $1.08 |
| 1 | R13 | 453 kΩ | Phos Vmon voltage divider | 0805 | 0.1% | ERA-6AEB4533V | Panasonic | $0.34 | $0.34 |

| | | | | | | | | | |
|---|---|---|---|---|---|---|---|---|---|
| 1 | R44 | 402 kΩ | MCP Vmon voltage divider | 0805 | 0.1% | ERA-6AEB4023V | Panasonic | $0.34 | $0.34 |
| 2 | R67, R68 | 324 kΩ | Snubber, 0.25W Resistor Automotive AEC-Q200, Pulse Withstanding Thick Film | 0805 | 0.5% | ERJ-PB6D3243V | Panasonic | $0.23 | $0.46 |
| 1 | R46 | 316 kΩ | MCP boost voltage divider | 0805 | 1% | RT0805FRE07316KL | Yageo | $0.23 | $0.23 |
| 2 | R58, R70 | 191 kΩ | Phos feedback voltage divider, MCP feedback voltage divider | 0805 | 0.1% | ERA-6AEB1913V | Panasonic | $0.36 | $0.72 |
| 1 | R16 | 140 kΩ | Phos boost voltage divider | 0805 | 0.1% | ERA-6AEB1403V | Panasonic | $0.43 | $0.43 |
| 14 | R7, R8, R14, R24, R26, R27, R31, R38, R39, R48, R55, R56, R60, R61 | 100 kΩ | Current sense, Boost feedback, Programmable input, Vmon | 0805 | 0.1% | RN73R2ATTD1003B50 | KOA Speer | $0.52 | $7.28 |
| 4 | R12, R20, R42, R54 | 50 kΩ | Boost compensation, Programmable input | 0805 | 0.1% | ERA-6AEB513V | Panasonic | $0.36 | $1.44 |
| 1 | R29 | 32.4 kΩ | Phos feedback voltage divider | 0805 | 0.1% | ERA-6AEB3242V | Panasonic | $0.55 | $0.55 |
| 1 | R41 | 16.7 kΩ | MCP current sense Rout | 0805 | 0.1% | TNPW080516K7BEEN | Vishay / Dale | $0.92 | $0.92 |
| 4 | R3, R18, R34, R49 | 10 kΩ | MOSFET gate voltage divider, Programmable input | 0805 | 0.05% | RN732ATTD1002A25 | KOA Speer | $0.43 | $1.72 |
| 4 | R5, R19, R36, R50 | 9 kΩ | RTCT timing resistor | 0805 | 0.1% | RT0805BRE079KL | Yageo | $0.54 | $2.16 |
| 1 | R69 | 5.9 kΩ | MCP feedback voltage divider | 0805 | 0.1% | ERA-6AEB5901V | Panasonic | $0.34 | $0.34 |
| 1 | R65 | 5 kΩ | Phos feedback voltage divider, MCP feedback voltage divider | 0805 | 1% | CRCW08055K00FKTA | Vishay / Dale | $0.15 | $0.15 |
| 7 | R6, R23, R30, R37, R52, R59, R63 | 1 kΩ | MOSFET current sense RC filter, Vmon3k divider | 0805 | 0.05% | ERA-6ARW102V | Panasonic | $0.71 | $4.97 |
| 4 | R2, R17, R32, R47 | 100 Ω | MOSFET gate voltage divider | 0805 | 0.1% | ERA-6VEB1000V | Panasonic | $0.70 | $2.80 |
| 2 | R22, R51 | 620 mΩ | Flyback MOSFET source current sense | 0805 | 1% | ERJ-U6QFR62V | Panasonic | $0.48 | $0.96 |
| 2 | R4, R35 | 100 mΩ | Boost MOSFET source current sense | 0805 | 0.5% | WSL0805R1000DEA | Vishay / Dale | $1.22 | $2.44 |
| 1 | C4 | 27 µF | Phos boost output capacitor, Energy storage, Tantalum wet | Axial | 10% | 135D276X9125F6E3 | Vishay / Tansitor | $56.59 | $56.59 |
| 3 | C19, C20, C31 | 10 µF | Boost output filtering caps, MLCC, 75Vdc | 1210 | 10% | GRM32EC72A106KE05L | Murata | $1.38 | $4.14 |
| 1 | C40 | 10 µF | Vdd energy storage capacitors, tantalum polymer, 20Vdc | 0805 | 20% | TCSP1D106M8R | ROHM Semiconductor | $1.05 | $1.05 |
| 13 | C39, C41, C42, C50, C51, C52, C53, C54, C55, C56, C57, C58, C59 | 1 µF | Boost input filtering cap, MLCC, 50Vdc | 0805 | 5% | CC0805JKX7R9BB105 | Yageo | $0.31 | $4.03 |
| 3 | C5, C36, C60 | 1 µF | Phos Boost 250V Ceramic Capacitor X7T | 1812 | 10% | CGA8P3X7T2E105K250KE | TDK Corporation | $1.80 | $5.40 |
| 4 | C1, C9, C16, C23 | 150 nF | MLCC, 50Vdc | 0805 | 5% | C0805C154J5RECAUTO | KEMET | $0.35 | $1.40 |
| | | | | | | | | | |
| 2 | C29, C30 | 4.7 nF | MCP HV Output Capacitor, 5kVdc, SMD | 2220 (5750) | 10% | 502S47W472KV4E | Johanson Dielectrics | $4.01 | $8.02 |
| 6 | C14, C45, C46, C47, C48, C49 | 3.3 nF | Phos HV Output Capacitor, 4kVdc, SMD | 1825 (4564) | 10% | HV1825Y332KXVATHV | Vishay / Vitramon | $2.00 | $12.00 |
| 4 | C2, C11, C17, C26 | 330 pF | RTCT Timing Cap, MLCC, 50Vdc | 0805 | 1% | C0805C331F5GACTU | KEMET | $1.05 | $4.20 |
| 6 | C3, C7, C10, C18, C22, C25 | 220 pF | MOSFET Source filter and Boost Comp | 0805 | 1% | VJ0805A221FXXCW1BC | Vishay / Vitramon | $0.44 | $2.64 |
| 8 | C6, C8, C13, C21, C24, C28, C61, C62 | 20 pF | Boost Comp, MLCC, 50Vdc | 0805 | 1% | C0805C200F5GACTU | KEMET | $1.10 | $8.80 |

| | | | | | | | | | |
|---|---|---|---|---|---|---|---|---|---|
| 4 | C12, C27, C43, C44 | 1pF | Snubber, 630V Ceramic Capacitor, Flyback Comp | 0805 | 50% | C0805C109DBGAC7800 | KEMET | $0.56 | $2.24 |
| 1 | J1 | MMDP-015 | Micro-D connector (15-pin, male) | -- | -- | MMDP-015-N00-WD6Q18.0-1-RH | Omnetics | $124.47 | $124.47 |
| 1 | -- | MMDS-015 | Micro-D connector (15-pin, female) | -- | -- | MMDS-015-N00-WD6Q18.0-1-RH | Omnetics | $128.50 | $128.50 |
| 2 | J2, J3 | 167-8626 | Circular high voltage hermetic connector | 0.5" d, 0.525" h | -- | | Teledyne/Reynolds | | |
| | | | | | | | | **Total:** | $6,254.98 |

Once the design, simulation, and bill of materials are finalized, printed circuit board (PCB) layout design begins. Allegro Design Entry CIS creates a netlist of the finalized circuit schematic which translates all the electrical connections to the layout editor. Allegro PCB Editor is chosen to design the layout of the PCB. Based on the size constraints, high voltage, and electromagnetic interference concerns, the MUVI PCB has four layers. The top and bottom layers house all the components while the second and third layers serve as a ground plane and high voltage plane, respectively.

Figure 5-1 shows the top layer of the PCB. This layer houses most of the components and traces. The control, power, and monitoring connections from the ICP as well as the two high voltage connections to the phosphor screen and microchannel plate are visible on the left of the PCB. The two power paths travel down the center of the PCB. The signal and control traces of the phosphor screen stages are located on the upper fourth of the board while the microchannel plate signal and control traces are located on the lower fourth of the board. This was done to isolate the power path from the control signals and to prevent them from coupling.

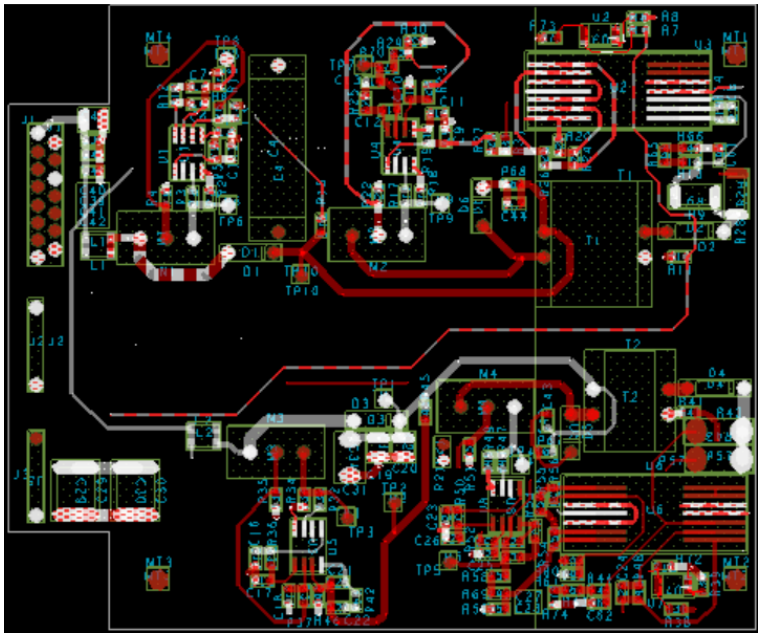

*Figure 5-1: Top Layer of the MUVI PCB*

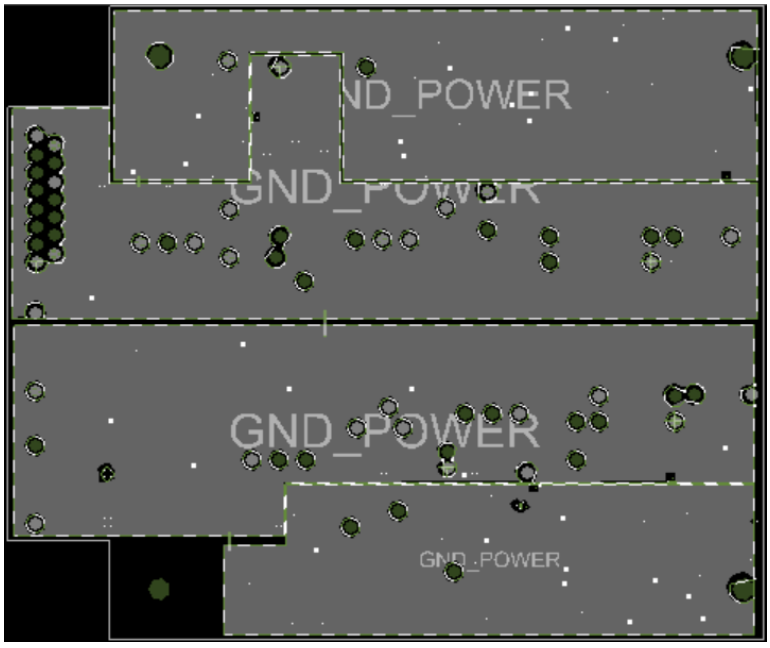


*Figure 5-2: MUVI Ground Layer*

Since MUVI utilizes a switching DC-DC converter, one can expect the switching node to generate unwanted electromagnetic interference. MUVI combats this problem using separate ground planes within the same layer. Ordered from top to bottom, Figure 5-2 shows the phosphor screen signal ground plane, the phosphor screen high voltage ground plane, the microchannel

plate high voltage ground plane, and the microchannel plate signal ground plane. The four separate ground planes are connected via thin traces. The thin traces prevent voltage fluctuations, located on the ground node of a high voltage output connection caused by the current switching between an on and off state, to reflect onto other parts of the circuit. The signal ground planes provide an accurate, steady reference voltage for the sensitive control and monitoring sections of the circuit. As shown in Figure 5-1, the signal and control traces for the phosphor screen and microchannel plate are located at the upper and lower areas of the board, respectively. Figure 5-2 shows the four separate ground planes that are connected via thin traces. One can see that the smaller two planes on the upper and lower portions of the board are signal grounds. These large ground planes shield the sensitive signal traces from the voltage fluctuations and electromagnetic interference emanating from the high voltage planes. The two large ground planes in the center of the board are for the phosphor screen and microchannel plate high voltage outputs. The planes utilize all available space to increase efficiency and maximize the electromagnetic shielding effect of the ground layer.

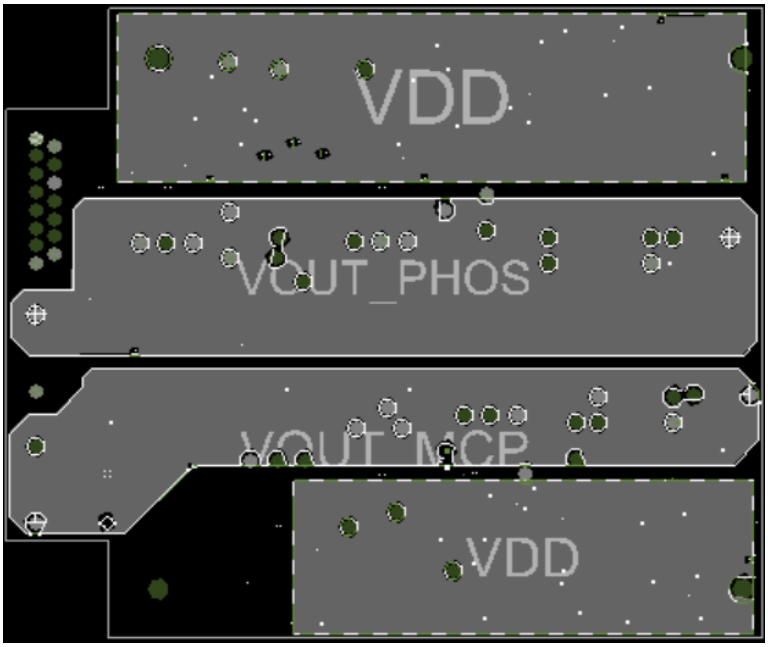


*Figure 5-3: MUVI High Voltage Layer*

The high voltage layer of the PCB, shown in Figure 5-3, contains the high voltage output planes and two smaller power planes. The smaller planes provide 13V to power all the integrated circuits. The high voltage planes have rounded corners to prevent catastrophic arcing from a high voltage plane to a different part of the circuit. Arcing can occur when charge accumulates around sharp edges of a high voltage conductor. Since the output current flows through the high voltage planes, increasing the size of the planes reduces the resistance of the power path. As a result, the efficiency of the converter increases. In addition to increased efficiency, the high voltage planes provide a safe, reliable solution to connect the high voltage flyback output, located on the right edge of Figure 5-1, to the high voltage output connectors, located on the left edge of Figure 5-1.

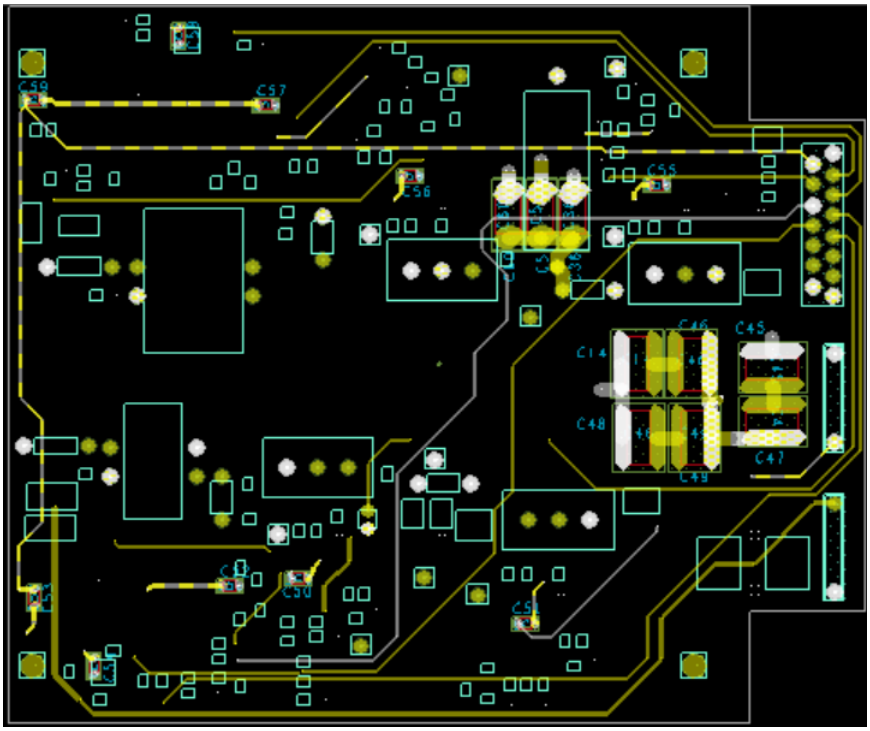


*Figure 5-4: Bottom layer of the MUVI PCB*

Figure 5-4 shows the bottom layer of the MUVI PCB. Since the location of the power path and control integrated circuits are relatively fixed due to size constraints, long traces are utilized to connect the feedback, voltage monitoring, current monitoring, and programmable input signals. The bottom layer of the PCB provides ample space for the long traces to travel the

full length of the board. To conserve space on the top layer, the phosphor screen output filter capacitors are placed on the bottom of the board.

Once layout design is complete, hardware testing begins. The first circuit tested is the custom transformer. The block diagram of the transformer test circuit can be seen in Figure 5-5. The primary side of the transformer was excited with a waveform generator producing a 1V sine wave with a frequency of 500 kHz. The transformer was designed to have a turns ratio of 1:15, thus a 15V sine wave shifted 180° is expected at the output. Figure 5-6 shows the results of the test. Channel 1 shows a 936mV sine wave on the primary side of the transformer and Channel 2 shows a 14.2V sine wave that has been shifted 180° on the secondary side of the transformer. Dividing 14.2 by 0.936 proves that the transformer has a turns ratio of 1:15.17 turns.

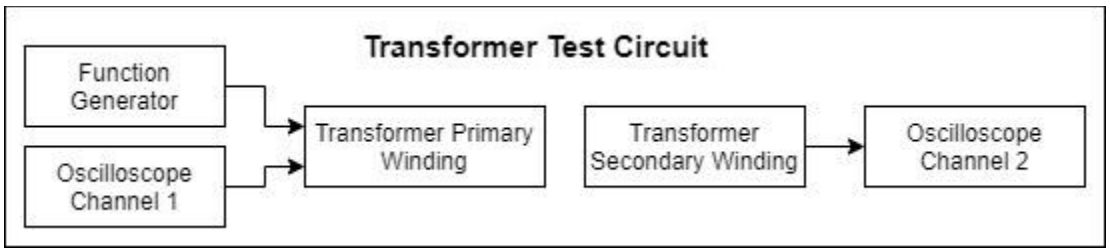


*Figure 5-5: Transformer test circuit*

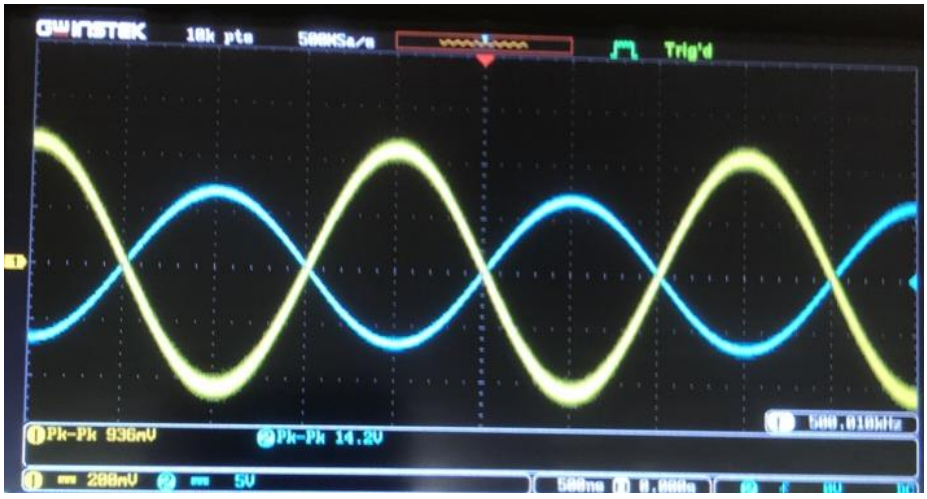


*Figure 5-6: Oscilloscope picture of the transformer test*

The next circuit tested is the output voltage monitoring circuit. To ensure the safety of those testing the circuit, the input voltage was reduced to 0V - 10V instead of the high voltage

flyback output. A different voltage divider made of two 10kΩ resistors was used to provide 0V -5V to the voltage follower circuit. Figure 5-7 shows the block diagram representation of the test circuit. The data shown in Figure 5-8 proves that the voltage monitoring circuit functions as expected.

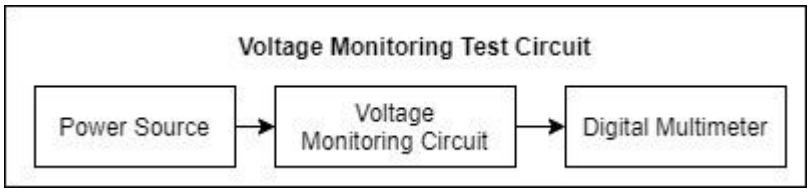


*Figure 5-7: Voltage Monitoring Test Circuit Block Diagram*

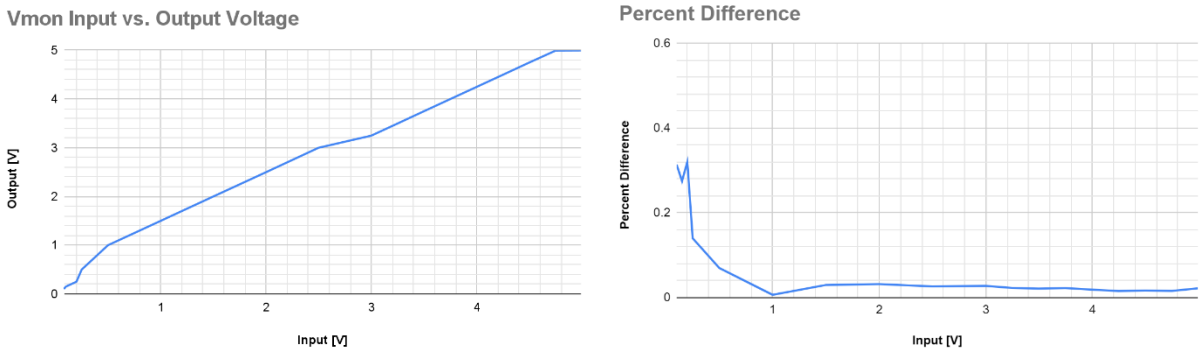


*Figure 5-8: a) Voltage monitoring input voltage vs output voltage b) Percent difference between the actual and expected output.*

The next circuit tested is the programmable input circuit. This circuit receives a control signal from the ICP ranging from 0V to -5V. The output of the programmable input circuit should linearly decrease from 2.5V to 0V as the input decreases from 0V to -5V. Figure 5-9 shows the programmable input test circuit block diagram and Figure 5-10 shows the collected data. One can see that Figure 5-10 matches the expected results.

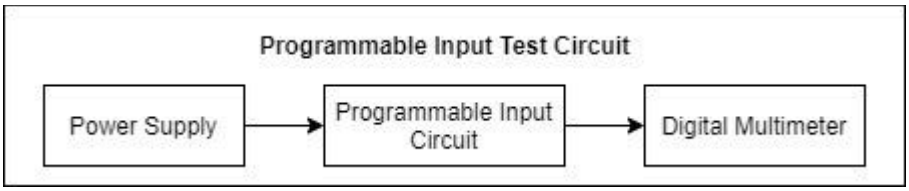

*Figure 5-9: Programmable Input Test Circuit Block Diagram*

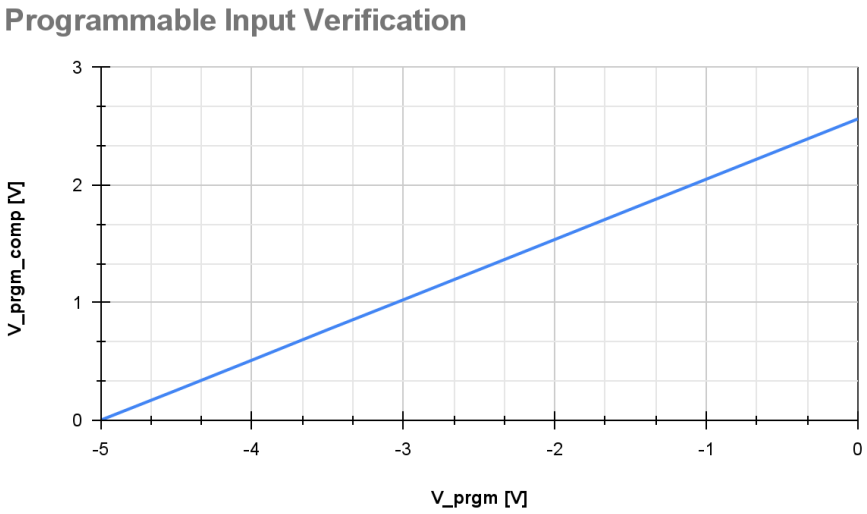


*Figure 5-10: Programmable input vs. output*

The next test is on the current sense circuit. Figure 5-11 shows the block diagram of the current sense test. The current sense circuit amplifies the voltage across the sense resistor and outputs the resulting value. Using Ohm's Law, one can calculate the voltage values across the sense resistor that correspond to current values ranging from 0A to 60µA. Then one can use a power supply to apply the calculated voltages across the sense resistor. As the current increases from 0A to 60µA, the output voltage should range from 0V to 5V. Figure 5-12 shows that the test results match the expected results.

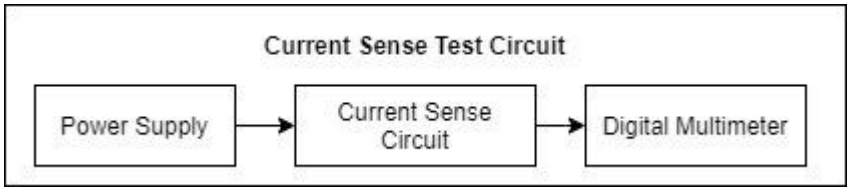


*Figure 5-11: Current Sense Test Circuit Block Diagram*

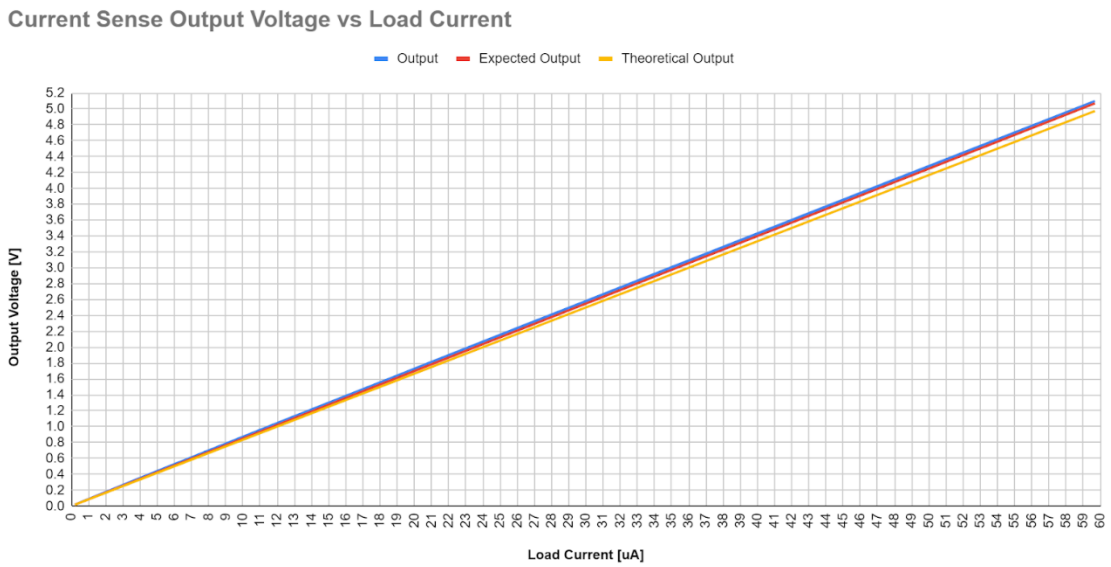


*Figure 5-12: Current sense output voltage VS the applied load current*

The final tests of the boost stage, flyback stage, and boost-flyback combinations will be conducted over the Summer of 2021. As a result, the experimental data will not be included in this report. The next chapter of the report will summarize the team's findings and present ideas for future design improvements.

# Chapter 6 - Conclusion

The simulation results show that a high voltage boost-flyback converter is a viable solution for the MUVI satellite. It provides two high voltage DC outputs to power the microchannel plate and phosphor screen within voltage ripple and accuracy specifications. The programmable input and output monitoring circuits were validated to work from the hardware tests in Chapter 5.

This project provides design inspiration for future projects that require a programmable input to linearly scale the high voltage output of a DC-DC converter. The solution is simple yet effective and offers an additional degree of freedom to control the output voltage. If a converter powers a sensitive load like the phosphor screen, then the programmable input circuit can be leveraged to slowly ramp up or down the output voltage during startup and shutdown conditions and prevent damage to the load.

The current design is limited by transformer size but the RM5 and RM6 cores were validated to fit within space requirements and provide the required 1:15 turns ratio for both flyback converters. The high voltage tests are scheduled for the upcoming Summer and the results will be included in next year's report.

Future design improvements can be made to the current monitoring circuit which will eliminate the RH6105 current sense amplifier and save board space. In the current design, the quad op-amp, OPA4277-SP, only uses three of the four available op-amps. Instead of leaving the fourth op-amp tied to ground, it can be used in a similar configuration to the voltage monitoring op-amp. The design uses the same shunt resistor connected between the load and ground but incorporates a non-inverting voltage amplifier with a filtering capacitor and compensation network. At maximum current the shunt resistor has a 1V drop across it and the op-amp

multiplies it by five just like the current sense amplifier. This improvement eliminates the need for a dedicated current sense amplifier and uses the fourth op-amp that is currently unused. Figure 6-1 shows the improved design and Figure 6-2 shows the simulation results for the microchannel plate load current varied between 0% and 100%.

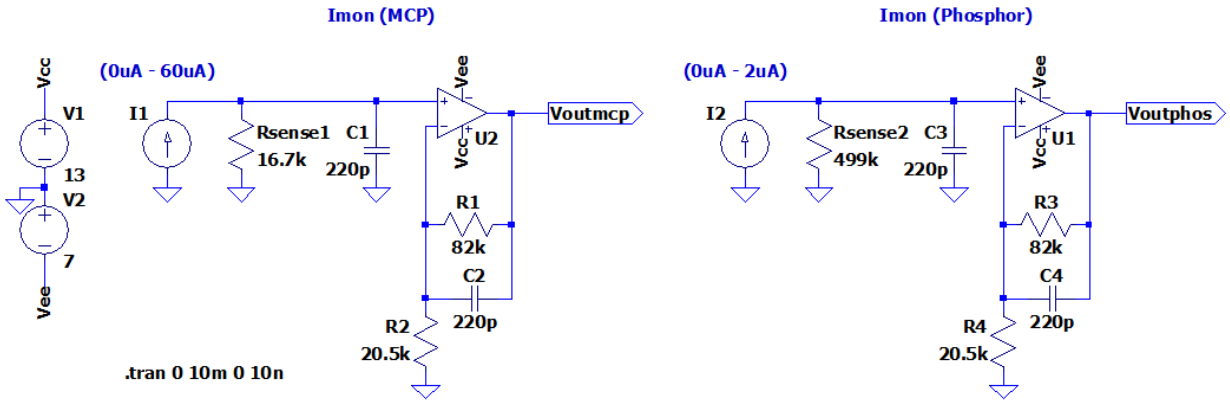


*Figure 6-1: Circuit schematic for the new current monitoring system of the microchannel plate*

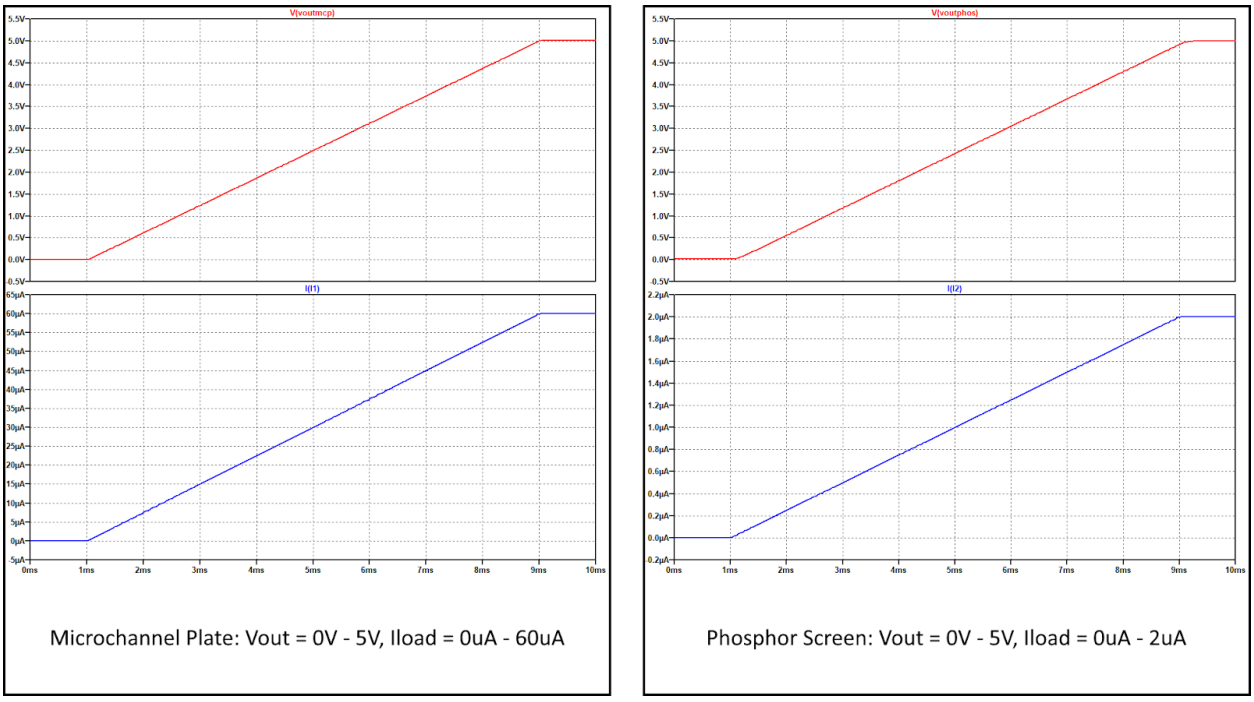


*Figure 6-2: Simulation results for the new current monitoring system*

The simulation results show that the same 0V to 5V voltage scaling can be achieved with the non-inverting op-amp setup. At 60µA load current the 16.7kΩ shunt resistor is 1V across and

the resistor ratio between R1 and R2 form the voltage gain of 5 to achieve up to 5V on the output. The results are nearly identical to the dedicated current sense amplifier. Removing the RH6105 from the design saves $794 and 30mm2 of space per board (15mm2 per IC).

# References


[1]. Taufik, *Introduction to Power Electronics*, Lulu Publishing, 2020.

[2]. D. Tiku, "History - DC Power Transmission," *IEEE Power & Energy Magazine*, Mar-2014. [Online]. Available: https://magazine.ieee-pes.org/marchapril-2014/history-12/. [Accessed: 30-Jan-2021].

[3]. L. James and J. Erbacher, "A brief history of power electronics and why it's important," *Power & Beyond*, 02-Nov-2020. [Online]. Available: https://www.power-and-beyond.com/a-brief-history-of-power-electronics-and-why-its-important-a-959053/. [Accessed: 30-Jan-2021].

[4]. M. Taufik, Taufik, and T. Wong, "Multiple-input single-output converter for renewable energy sources", Proc. of IEEE Symposium on Industrial Electronics and Applications, pp. 130-135, September 2012.

[5]. Taufik, K. Htoo, and G. Larson, "Multiple-input bridge converter for connecting multiple renewable energy sources to a DC system", Proc. of Future Technologies Conference, pp. 444-449, December 2016.

[6]. Taufik, T. Wong, O. Jong, and D. Dolan, "Design and simulation of multiple-input single-output DC-DC converter", Ninth International Conference on Information Technology-New Generations, pp. 478-483, April 2016.

[7]. Taufik and M. Muscarella, "Development of DC house prototypes as demonstration sites for an alternate solution to rural electrification", Sixth International Annual Engineering Seminar, pp. 262-265, August 2016.

[8]. Taufik and M. Taufik, "The DC House Project: Promoting the use of renewable energy for rural electrification", International Conference on Power Engineering and Renewable Energy, pp. 1-4, July 2012.

[9]. Taufik, R. Prasetyo, D. Dolan, and D. Garinto, "A new multiphase multi-interleaving buck converter with bypass LC", 36th Annual Conference on IEEE Industrial Electronics Society, pp. 291-295, November 2011.

[10]. Taufik, *Advanced Power Electronics*, Lulu Publishing, 2021.

[11]. N. Weiser, "Dual High-Voltage Power Supply for use On Board a CubeSate", M.S. Thesis, EE, Cal Poly, San Luis Obispo, California, 2014. Accessed on: Feb. 23, 2021. [Online]. Available: https://digitalcommons.calpoly.edu/theses/1204/

[12]. A. H. Weinberg and J. Schreuders, "A High-Power High-Voltage DC-DC Converter for Space Applications," in *IEEE Transactions on Power Electronics*, vol. PE-1, no. 3, pp. 148-160, July 1986, doi: 10.1109/TPEL.1986.4766299.

[13]. Q. Tong and D. Zhang, "Research on a high output current DC/DC converter with wide input voltage range for space applications," 2016 International Conference on Integrated Circuits and Microsystems (ICICM), Chengdu, China, 2016, pp. 205-209, doi: 10.1109/ICAM.2016.7813593.

[14]. S. Park, A. Goldin and J. Rivas-Davila, "Miniature High-Voltage DC-DC Power Converters for Space and Micro-Robotic Applications," *2019 IEEE Energy Conversion Congress and Exposition (ECCE)*, Baltimore, MD, USA, 2019, pp. 2007-2014, doi: 10.1109/ECCE.2019.8913249.

[15]. K. Rider, MUVI PowerPoint Presentation, Topic: "High Voltage Power Supply (HVPS) Project", UC Berkely Space Sciences Laboratory, Berkely, California, Sept. 18, 2020.

[16]. I. Mathur, "High Performance Liquid Rocket Propellant," 14-Apr-2015.

[17]. I. R. Dutton, "Engineering code of ethics," in IEEE Potentials, vol. 9, no. 4, pp. 30-31, Dec. 1990, doi: 10.1109/45.65865.

[18]. R. Langley, "GPS, the Ionosphere, and the Solar Maximum," University of New Brunswick, Tech Report, July 2000.

[19]. M. Forouzesh, Y. P. Siwakoti, S. A. Gorji, F. Blaabjerg and B. Lehman, "Step-Up DC–DC Converters: A Comprehensive Review of Voltage-Boosting Techniques, Topologies, and Applications," in IEEE Transactions on Power Electronics, vol. 32, no. 12, pp. 9143-9178, Dec. 2017, doi: 10.1109/TPEL.2017.2652318.

# Appendix A. Senior Project Analysis

Title: MUVI Satellite High Voltage Power Supply Design

Student Names: Nicholas Palmer & Jason Heil

Advisor Name: Dr. Taufik

- Summary of Functional Requirements

The Miniaturized Ultraviolet Imager (MUVI) functions as an imager that records pictures from the ionosphere of the Earth. Data from MUVI assists scientists in making predictions of when and where electromagnetic interference may occur from space. MUVI finished the redesign of the power supply in its fourth year of development. Strict size constraints exist on MUVI because it must fit in a 2U, CubeSat module. The high voltage power supply delivers power to the phosphor screen of the imager as well as the microchannel plate (MCU). Voltage and current monitoring lines link the output of the phosphor screen and microchannel plate to the instrument control panel (ICP). The ICP of MUVI supplies the control signals to the high voltage power supply.

- Primary Constraints

The two most difficult challenges in designing the high voltage power supply (HVPS) of MUVI include the small physical size of the device and the requirement that it operates in the vacuum of space. MUVI intends to replace an older satellite called the Ionosphere Connection Explorer (ICON). ICON's large size made it difficult and expensive to send to space. MUVI solves this problem by adhering to the CubeSat standards and therefore can ride on NASA's

CubeSat rockets. The printed circuit board area does not exceed 3.64” width x 3.52” length. The component height does not exceed 0.35” directly underneath the imager and 0.91” in front of the imager. The small size increases the likelihood of electromagnetic interference from the switching components of the DC-DC converter and increases the chance of arcing between high voltage portions of the circuit. The low pressure of space increases the chances of arcing between high voltage components.

- Economic

The human capital supplied to build the HVPS originates from the manufactures of the integrated circuit chips in factories. The final assembly of the MUVI occurs at the Space Sciences Laboratory (SSL) of UC Berkeley. NASA supplies most of the financial capital to fund the project. SSL and NASA jointly fund the redesign of the HVPS. The manufactured capital of SSL includes all the tooling included to manufacture and assemble the MUVI. Once SSL manufactures the tooling, they can continue to create many MUVIs. MUVI requires several different natural resources including iron, silicone, and phosphor. SSL does not intend to make thousands of satellites, so the impact of MUVI remains small. The most environmentally costly part of MUVI includes the large amount of energy required to send the satellites to space.

Costs accrue during the project planning and design period because of the billable hours that the engineers work. Design and simulation software also increase the cost of the project. When engineers finish the design, the real components and testing equipment verify the functionality of the design. Finally, full manufacturing and assembly can occur and MUVI can begin accruing benefits. NASA intends to purchase the MUVI assemblies and is the main customer.

The project requires both financial and human capital to succeed. NASA supplies the financial investment into the project. A team of Cal Poly engineers, with a team of SSL engineers, supplies the human capital and design effort for the project. Initial cost estimates of the project predict that MUVI should cost about $15,000. The cost of the project includes all software, hardware, and work hours that the project requires.

The project profits are based on the number of units sold to the final customer. NASA intends to send a fleet of 14 to 15 units to space to collect data. A final design of the MUVI high voltage power supply must be submitted by the middle of February. The manufacturing of the MUVIs begins in the middle of April. The products are expected to last several years because of the difficulty of doing maintenance in space.

TABLE A-1: MUVI POWER SUPPLY COST ESTIMATES

| Item | Optimistic Price | Adjusted Price | Justification |
|---|---|---|---|
| Circuit Components | $450 | $600 | Preliminary design from UC Berkeley has 14 op-amps at ~$11 each (from Digikey), 2 CMOS switching stages, 2 voltage multiplier ICs, and various resistors + capacitors. Adjusted price reflects obtaining additional/replacement parts for V2 and V3 build + test cycles.<br><br>Optimistic price = $450<br>Realistic price = $600<br>Pessimistic price = $750<br>Adjusted price = ($450 + 4×$600 + 750) / 6 = $600 |
| Pspice + Allegro Licensing Fees | $3,000 | $3,000 | This price reflects the licensing fees for Pspice (circuit design) and Allegro (pcb design) software. The power lab computers at Cal Poly have both applications installed. |
| Design Labor | $9,600<br><br>($4,800 per team member) | $11,200<br><br>($5,600 per team member) | Derived from a rate of $30/hour, 6 hours/week, for 20 weeks. Adjusted price allocates an extra 20 hours for last-minute changes over the duration of the project.<br><br>Optimistic hours = 120 hours/person<br>Realistic hours = 140 hours/person<br>Pessimistic hours = 160 hours/person<br>Adjusted hours = (120 + 4×140 + 160) / 6 = 140 hours<br>Adjusted price = 140 hours × $40/hour = $5,600 |
| Senior Project Publication Fee | $12 | $12 | This fee covers the Cal Poly Digital Commons publication fee for senior projects. |
| Final Presentation Poster | $20 | $25 | Tri-fold poster costs $15. Printing pictures, graphs, and using various adhesives costs $5. Adjusted cost covers emergency reprinting.<br><br>Optimistic price = $20<br>Realistic price = $25<br>Pessimistic price = $30<br>Adjusted price = ($20 + 4×$25 + $30) / 6 = $25 |
| | **Total:** | **$14,837** | |

## TABLE A-2: FINAL EE 461 – EE 462 GANTT CHART

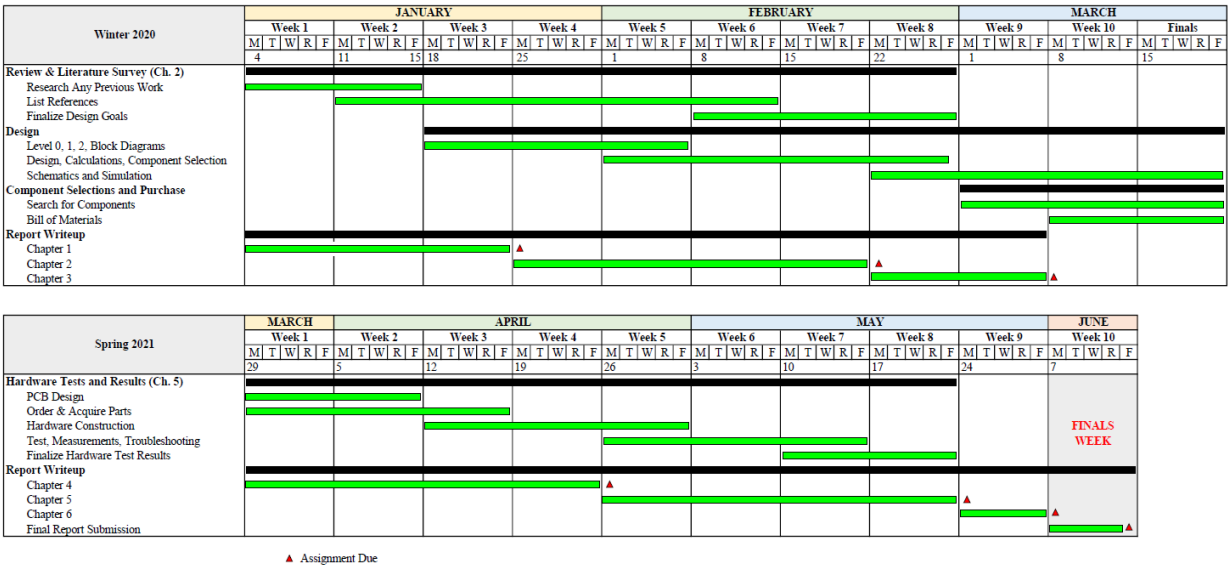


## TABLE A-3: FINAL MUVI BILL OF MATERIALS

| Count | Reference Designator | Value | Description | Size | Tolerance | Part Number | Manufacturer | Per Unit Cost [$] | Per Board Cost [$] |
|---|---|---|---|---|---|---|---|---|---|
| 4 | U1, U4, U5, U8 | ISL71043MBZ | Rad Hard Boost/Flyback PWM Controller | SOIC-8 | -- | ISL70143MBZ | Renesas | $290.37 | $1,161.48 |
| 2 | U3, U7 | RH6105 | Rad Hard Current Sense Amplifier | MSOP-8 | -- | RH6105 | Analog Devices | $397.00 | $794.00 |
| 2 | U2, U6 | OPA4277-SP | Rad Hard Quad Op-Amp | CFP-14 | -- | OPA4277-SP | Texas Instruments | $950.40 | $1,900.80 |
| 4 | M1, M2, M3, M4 | IRHM7460SE | Rad Hard NMOS, 500Vds | TO-254AA | -- | IRHM7460SE | International Rectifier | | |
| 2 | D1, D3 | JAN1N5614US | Rad Hard Diode, 200Vbr (Boost) | Axial | -- | JAN1N5614US | Microsemi | $12.86 | $25.72 |
| 2 | D2, D4 | JANTX1N6526 | Rad Hard Diode, 7500Vbr (Flyback) | Axial | -- | JANTX1N6526 | doEEEt | $542.90 | $1,085.80 |
| 2 | D5, D6 | JANTX1N5618 | Transformer Snubber Diodes, 600Vbr | Axial | -- | JANTX1N5618 | SemTech | $310.10 | $620.20 |
| 1 | R21 | 11029759-00 | Rad Hard Thermistor | Axial | -- | 11029759-00 | Measurement Specialties | $237.14 | $237.14 |
| 2 | T1, T2 | -- | 1:15 Step-up Transformer | RM5 / RM6 | -- | -- | -- | -- | -- |
| 2 | L1, L2 | 250 µH | Boost Inductor | 4.5mm x 4.5mm x 3mm | 25% | 744235251 | Würth Electronic | $1.43 | $2.86 |
| 2 | R9, R28 | 500 MΩ | Phos Vmon and flyback voltage divider | 2010 | 0.5% | HVCB2010DDC500M | Stackpole Electronics | $9.25 | $18.50 |
| 2 | R43, R57 | 200 MΩ | MCP Vmon and flyback voltage divider | 2512 | 1% | HVCB2512FDD200M | Stackpole Electronics | $7.59 | $15.18 |
| 3 | R15, R25, R45 | 5.1 MΩ | Phos flyback compensation, Boost divider | 0805 | 1% | RC0805FR-075M1L | Yageo | $0.13 | $0.39 |
| 1 | R53 | 2 MΩ | MCP flyback compensation | 0805 | 1% | ERJ-6ENF2004V | Panasonic | $0.10 | $0.10 |
| 3 | R11, R72, R73 | 499 kΩ | MCP current sense Rout, Phos Rsense, Phos Rout | 0805 | 0.1% | 6AEB4993V | Panasonic | $0.36 | $1.08 |
| 1 | R13 | 453 kΩ | Phos Vmon voltage divider | 0805 | 0.1% | ERA-6AEB4533V | Panasonic | $0.34 | $0.34 |
| 1 | R44 | 402 kΩ | MCP Vmon voltage divider | 0805 | 0.1% | ERA-6AEB4023V | Panasonic | $0.34 | $0.34 |
| 2 | R67, R68 | 324 kΩ | Snubber, 0.25W Resistor Automotive AEC-Q200, Pulse Withstanding Thick Film | 0805 | 0.5% | ERJ-PB6D3243V | Panasonic | $0.23 | $0.46 |
| 1 | R46 | 316 kΩ | MCP boost voltage divider | 0805 | 1% | RT0805FRE07316KL | Yageo | $0.23 | $0.23 |
| 2 | R58, R70 | 191 kΩ | Phos feedback voltage divider, MCP feedback voltage divider | 0805 | 0.1% | ERA-6AEB1913V | Panasonic | $0.36 | $0.72 |

| | | | | | | | | | |
|---|---|---|---|---|---|---|---|---|---|
| 1 | R16 | 140 kΩ | Phos boost voltage divider | 0805 | 0.1% | ERA-6AEB1403V | Panasonic | $0.43 | $0.43 |
| 14 | R7, R8, R14, R24, R26, R27, R31, R38, R39, R48, R55, R56, R60, R61 | 100 kΩ | Current sense, Boost feedback, Programmable input, Vmon | 0805 | 0.1% | RN73R2ATTD1003B50 | KOA Speer | $0.52 | $7.28 |
| 4 | R12, R20, R42, R54 | 50 kΩ | Boost compensation, Programmable input | 0805 | 0.1% | ERA-6AEB513V | Panasonic | $0.36 | $1.44 |
| 1 | R29 | 32.4 kΩ | Phos feedback voltage divider | 0805 | 0.1% | ERA-6AEB3242V | Panasonic | $0.55 | $0.55 |
| 1 | R41 | 16.7 kΩ | MCP current sense Rout | 0805 | 0.1% | TNPW080516K7BEEN | Vishay / Dale | $0.92 | $0.92 |
| 4 | R3, R18, R34, R49 | 10 kΩ | MOSFET gate voltage divider, Programmable input | 0805 | 0.05% | RN732ATTD1002A25 | KOA Speer | $0.43 | $1.72 |
| 4 | R5, R19, R36, R50 | 9 kΩ | RTCT timing resistor | 0805 | 0.1% | RT0805BRE079KL | Yageo | $0.54 | $2.16 |
| 1 | R69 | 5.9 kΩ | MCP feedback voltage divider | 0805 | 0.1% | ERA-6AEB5901V | Panasonic | $0.34 | $0.34 |
| 1 | R65 | 5 kΩ | Phos feedback voltage divider, MCP feedback voltage divider | 0805 | 1% | CRCW08055K00FKTA | Vishay / Dale | $0.15 | $0.15 |
| 7 | R6, R23, R30, R37, R52, R59, R63 | 1 kΩ | MOSFET current sense RC filter, Vmon3k divider | 0805 | 0.05% | ERA-6ARW102V | Panasonic | $0.71 | $4.97 |
| 4 | R2, R17, R32, R47 | 100 Ω | MOSFET gate voltage divider | 0805 | 0.1% | ERA-6VEB1000V | Panasonic | $0.70 | $2.80 |
| 2 | R22, R51 | 620 mΩ | Flyback MOSFET source current sense | 0805 | 1% | ERJ-U6QFR62V | Panasonic | $0.48 | $0.96 |
| 2 | R4, R35 | 100 mΩ | Boost MOSFET source current sense | 0805 | 0.5% | WSL0805R1000DEA | Vishay / Dale | $1.22 | $2.44 |
| 1 | C4 | 27 µF | Phos boost output capacitor, Energy storage, Tantalum wet | Axial | 10% | 135D276X9125F6E3 | Vishay / Tansitor | $56.59 | $56.59 |
| 3 | C19, C20, C31 | 10 µF | Boost output filtering caps, MLCC, 75Vdc | 1210 | 10% | GRM32EC72A106KE05L | Murata | $1.38 | $4.14 |
| 1 | C40 | 10 µF | Vdd energy storage capacitors, tantalum polymer, 20Vdc | 0805 | 20% | TCSP1D106M8R | ROHM Semiconductor | $1.05 | $1.05 |
| 13 | C39, C41, C42, C50, C51, C52, C53, C54, C55, C56, C57, C58, C59 | 1 µF | Boost input filtering cap, MLCC, 50Vdc | 0805 | 5% | CC0805JKX7R9BB105 | Yageo | $0.31 | $4.03 |
| 3 | C5, C36, C60 | 1 µF | Phos Boost 250V Ceramic Capacitor X7T | 1812 | 10% | CGA8P3X7T2E105K250KE | TDK Corporation | $1.80 | $5.40 |
| 4 | C1, C9, C16, C23 | 150 nF | MLCC, 50Vdc | 0805 | 5% | C0805C154J5RECAUTO | KEMET | $0.35 | $1.40 |
| 2 | C29, C30 | 4.7 nF | MCP HV Output Capacitor, 5kVdc, SMD | 2220 (5750) | 10% | 502S47W472KV4E | Johanson Dielectrics | $4.01 | $8.02 |
| 6 | C14, C45, C46, C47, C48, C49 | 3.3 nF | Phos HV Output Capacitor, 4kVdc, SMD | 1825 (4564) | 10% | HV1825Y332KXVATHV | Vishay / Vitramon | $2.00 | $12.00 |
| 4 | C2, C11, C17, C26 | 330 pF | RTCT Timing Cap, MLCC, 50Vdc | 0805 | 1% | C0805C331F5GACTU | KEMET | $1.05 | $4.20 |
| 6 | C3, C7, C10, C18, C22, C25 | 220 pF | MOSFET Source filter and Boost Comp | 0805 | 1% | VJ0805A221FXXCW1BC | Vishay / Vitramon | $0.44 | $2.64 |
| 8 | C6, C8, C13, C21, C24, C28, C61, C62 | 20 pF | Boost Comp, MLCC, 50Vdc | 0805 | 1% | C0805C200F5GACTU | KEMET | $1.10 | $8.80 |
| 4 | C12, C27, C43, C44 | 1pF | Snubber, 630V Ceramic Capacitor, Flyback Comp | 0805 | 50% | C0805C109DBGAC7800 | KEMET | $0.56 | $2.24 |
| 1 | J1 | MMDP-015 | Micro-D connector (15-pin, male) | -- | -- | MMDP-015-N00-WD6Q18.0-1-RH | Omnetics | $124.47 | $124.47 |
| 1 | -- | MMDS-015 | Micro-D connector (15-pin, female) | -- | -- | MMDS-015-N00-WD6Q18.0-1-RH | Omnetics | $128.50 | $128.50 |
| 2 | J2, J3 | 167-8626 | Circular high voltage hermetic connector | 0.5" d, 0.525" h | -- | | Teledyne/Reynolds | | |
| | **Total** | | | | | | | | $6,254.98 |

- If Manufactured on a Commercial Basis

The MUVI device intends to be manufactured on a commercial basis. NASA intends to purchase 14 to 15 devices over the first two years of development. Because of the strict space and CubeSat ratings, the estimated manufacturing cost remains high during full production. After verification of the design, the estimated manufacturing cost remains about $4,000. We predict that the final cost of the MUVI to the customer ranges between $10,000 and $12,000. If 14 to 15 devices sell annually, estimated profits per year exceed $112,000. Once the system reaches space, the only costs to the customer include maintaining communication with the device.

- Environmental

The largest environmental impacts created by MUVI include the large amount of resources required to send MUVI to space and the silicone components used in the high voltage power supply. The fuel used to thrust the satellite into space releases large amounts of greenhouse gasses into the environment. Before burning the fuel, it must go through a refining process [16]. The refining process also releases large amounts of greenhouse gasses and consumes power from the utility provider. The manufacturing and testing phase requires multiple HVPS. Waste associated with testing increases as the number of tests performed increases. Since each MUVI only requires one trip to space and the long lifespan of the device, MUVI has a relatively low environmental impact. Since MUVI travels to space, the damaged ecosystem includes space. Space has a large number of decommissioned or broken satellites. As more satellites become obsolete, the amount of space debris increases. Removing space debris remains difficult, so broken satellites must be avoided.

- Manufacturability

The largest challenges associated with manufacturing the MUVI include maintaining a clean environment so as to not compromise its performance. Workers must assemble the sensitive components of MUVI in a clean room environment. Clean rooms are difficult and costly to maintain. This greatly increases the cost of assembly of MUVI. Because of the difficulty associated with maintenance in space, MUVI must use the best rated materials that function in the harsh environment of space. The material must not need maintenance for the entire life of the MUVI mission.

- Sustainability

Once the device reaches space, maintenance becomes nearly impossible. As a result, only the highest quality materials and components go into the manufacturing of MUVI. If MUVI fails while in space, the satellite will be useless and become space debris. Ensuring MUVI uses materials rated for space provides the best assurance that MUVI has a long lifespan. Improving the lifespan of the mission improves the sustainability of MUVI because less satellites must travel to space. The resources used in the manufacturing of MUVI must come from sustainable sources or risk to the natural environment exists. Increasing the switching speed of the DC-DC converter increases the efficiency of the device. The large electromagnetic interference associated with increasing the switching speed of the DC-DC converters makes it difficult to upgrade the design.

- Ethical

The MUVI project faces and overcomes ethical challenges found in the IEEE Code of Ethics [17] and from a utilitarianism standpoint. The IEEE Code of Ethics states this project

complies with “ethical design and sustainable development practices.” The MUVI power supply achieves this through extensive simulation of design approaches before building any physical circuits. This cuts down on the amount of parts wasted in the iterative design process. Reducing waste actively contributes to sustainability through reducing additional part shipment, reducing associated greenhouse gasses with manufacturing, and fewer components sent to the landfill. Other ethical challenges include conflict of interest, bribery, properly crediting others’ work, and accepting honest criticism of technical work. The engineering team takes additional precaution in protecting intellectual property through limiting who has access to electrical designs. Project information is kept strictly between team members in encrypted storage on the internet to prevent outside parties from gaining access to sensitive intellectual property. This document and all subsequent documentation aim to cite and credit all contributors using the IEEE citation format to further credibility and legitimacy of this project. MUVI provides a learning opportunity for project planning and design. As students, our responsibility lies in learning from mistakes and honest criticism from more experienced engineers. Our commitment to lifelong learning includes taking feedback to improve the design and integrity of the project.

From a utilitarianism standpoint, MUVI provides an opportunity to further humanity’s understanding of the ionosphere and its effect on communications on Earth. Understanding how the ionosphere affects communications can lead to technologies that reduce interference and increase stability in day-to-day operations. Sensitive data transmission happens during all hours of the day and signal corruption and disruption can lead to devastating consequences. GPS communications are affected by ionosphere weather patterns in the form of signal delay and reduced positioning accuracy [18].

- Health and Safety

The strict CubeSat and NASA standards of spaceflight ensure the safety of all those impacted by MUVI. Design feedback and reviews provide crucial safety checks to prove that the system will not harm anyone during its design, manufacturing, and operation. The largest safety concern occurs during the launch and flight of the MUVI satellite to space. The large amount of energy and small margin of error makes any flight to space a dangerous operation. NASA takes the responsibility to provide a safe flight to space. Health and safety benefits include the knowledge of when the ionosphere produces large electromagnetic interference. This interference can disrupt large portions of our society that depend on electrical infrastructure such as communication systems. The loss of communication systems can interfere with the police and medical services to maintain the public's safety. Therefore, having knowledge of when and where electromagnetic interference will occur increases public safety.

- Social and Political

Social and political issues involved with the design, manufacturing, and deployment of MUVI include the issue of who has access to the data that MUVI collects. Many people may believe that the information collected from space belongs to all those who request access. Conversely, NASA argues that they funded the project and provided transportation to space, therefore, they should remain the sole recipient of the data collected. The direct stakeholders include NASA and SSL. NASA provides most of the funding for the project while SSL does the testing and manufacturing of the devices. Indirect stakeholders include the average citizen of the United States. NASA intends to use the information gathered from MUVI to predict where and when high energy ionized radiation may arrive from space. The ionized radiation has the potential to disable sensitive electrical equipment such as communication systems. If NASA can

predict where and when the ionized radiation arrives with sufficient warning, society can take steps to protect the vulnerable equipment before damage occurs.

NASA and SSL benefit equally from the project, because they both receive the data that MUVI collects. From the beginning, NASA has provided most of the funding for the project while SSL provides testing and manufacturing capabilities. The project benefits stakeholders by improving the reputation of each company additionally the data acquired that helps the scientists to improve the world. The project may harm the stakeholders, if a catastrophic failure happens at takeoff or if the scientists cannot use the data acquired. The project can create inequalities between stakeholders, if the scientists do not share their data and analysis with the public. If NASA supplies the analysis to the public in an easy to understand format, those who have a technical background and those who do not will all benefit. NASA must ensure that the average person benefits from the information gathered by MUVI.

- Development

New skills learned to develop this project include DC-DC converter design and simulation, component selection for high voltage space applications, and Allegro PCB design software. Computers in the power electronics lab provided access to full versions of OrCAD and Allegro design tools throughout the design process. Extensive simulations improved PSPICE skills and taught how to simulate a large complex circuit. Reading the literature search documents gave a better understanding of how to read large technical documents while quickly extracting the pertinent information. The literature search assisted in understanding the requirements of space rated, radiation hardened components used in the ICON high voltage power supply [19]. Weekly team meetings provided consistent updates and focused research efforts.